

ACTA TECHNICA JAURINENSIS

Vol. 17, No. 3, pp. 104-110, 2024 10.14513/actatechjaur.00743



Research Article

Sawmill scheduling: an application-oriented model

Csaba Kebelei¹, Mate Hegyhati^{1,*}

¹ University of Sopron Bajcsy-Zs. u. 4, H9400 Sopron, Hungary *e-mail: hegyhati.mate@uni-sopron.hu

Submitted: 10/2/2024 Accepted: 17/07/2024 Published online: 30/07/2024

Abstract:

Sawmills play a key role in the primary sector of the wood industry producing lumber from tree logs through a multi-stage process including inspections, classification, sawing, drying, etc. The sawing step can become a bottleneck due to the high investment costs the necessary equipment present. Thus, their schedule can be of significant economic importance, resulting in several studies over the years. While most of the approaches in the literature consider a simple model of production and focus on the stochastic nature of real-life problems, present work details a more in-depth model to better tackle practical considerations of less automated and smaller sawmills. The proposed Mixed-Integer Linear Programming model addresses volatile labour availability and differences between the two most dominant sawing technologies. The efficiency of the model is tested on randomly generated instances. The proposed approach can provide the optimal solution within reasonable time for short-term instances.

Keywords: sawmill; scheduling; optimization; timber industry

I. INTRODUCTION AND LITERATURE REVIEW

As sustainability becomes an increasingly pressing issue, the application of renewable materials gains ever growing focus. Wood is one of nature's CO2 sequestration technologies, and the timber industry plays a key role in producing products that can store the captured carbon in the long-term. However, the widespread application of wood-based products requires not only feasible technologies and sufficient quality. The whole value chain of these products must be financially competitive to that of other nonrenewable options such as plastic. As a result, improving the efficiency of the supply chain and each individual facility can be vital to real-life adaptation.

While many works in the literature focus on highlevel optimization of supply chains in the wood industry [1, 2, 3], present work addresses the optimal operation of sawmills that play a key role in the primary wood industry. Sawmills are responsible to produce various primary wood products such as lumber and plank from unprocessed wood logs. The production process is a complex sequence of steps from inspection and classification via the actual sawing to various treatments as shown Fig. 1. Sawing equipment present a significant cost of investment in such facilities, thus, their optimized

utilization is of importance for the overall efficiency of the plant.

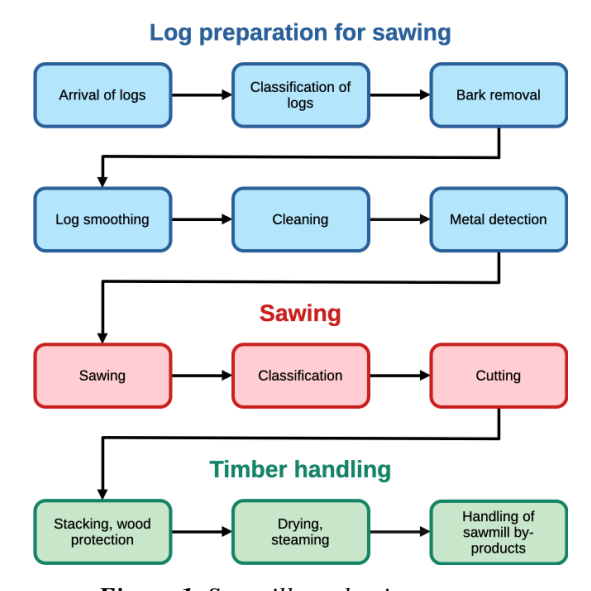


Figure 1. Sawmill production process

The decision flexibility of the production planner is the selection of log classes to be processed and the applied cutting pattern for the span of the entire time horizon. Optimization of cutting pattern is another well-researched field [4] whose goal is generally to minimize waste. At this stage of production

planning, it is assumed that the list of cutting patterns to apply are determined a-priori. Each pattern is applicable to a different log class with a specific range of diameter and yields different quantities of various products. An example for such a cutting pattern is shown in **Fig. 2**.

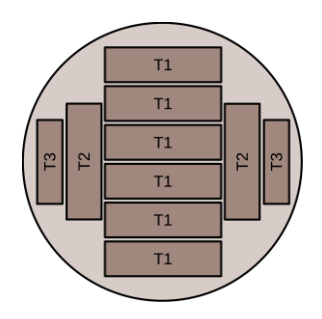


Figure 2. Cutting pattern example

Cost-optimal planning of the sawing step was first examined by [5], where the time horizon was split to intervals and subintervals. For each subinterval, the model could determine the portion of that time allocated for each cutting pattern. The objective was to minimize the cost consisting of both late or missed deliveries and storage. The presented model considered only a single cutting pattern for each log class, a single saw, and deterministic behaviour. This model has been extended and generalized many times in the literature. In [6] and [7] the possibility for deciding the cutting pattern for the logs with the same diameter were introduced, while [8] extended the model to address multiple sawing equipment. Another direction of research focused incorporating non-deterministic behaviour into the optimization process, mostly via robust scheduling as presented in [9] and [10].

All of these models, however, consider a simplified, high-level model of the sawing procedure itself, as a single-stage continuous process. This estimation is adequate for high level planning, and precise enough for highly automated sawmills with huge annual throughput. However, as the scale of the facility decreases, technological details become more prevalent, providing the motivation for the proposed investigation and model of this work.

II. MOTIVATION AND PROBLEM DEFINITION

Sawmills show vast variety in both scale and the age or modernity of equipment. Large-scale facilities tend to be highly automated requiring minimal human interventions for either its operation or material movement. On the other end of the spectrum, family-owned small businesses tend to have older equipment whose operation requires more human work both for moving the logs and lumbers and for the operation of saws. Moreover, special domain specific knowledge is needed for issues like the ideal positioning of logs, avoiding defects, etc.,

which are overcome by cutting-edge sensors and actuators at their modernized counterparts. From the modelling point of view, high-volume facilities with modern equipment can be adequately addressed as a single-stage continuous process, sometimes with optional setup times. For this case, simple linear scheduling models can provide sufficient accuracy. For small-scale facilities, many assumptions of these models are not met. In this work we address some of these, as a first step towards a more process specific model.

One key domain specific feature not addressed in literature models is the basic technology used for sawing. While new techniques are being developed at several companies, often mixing previous ideas and new innovations in sensor technology, robotics, and artificial intelligence [8, 9], most existing equipment can be categorized into two major groups: frame saws and band saws. Frame saws have been around for a long time and are ideal when many logs of the same size are to be sawed with a plain cutting pattern. The saw operates several bands in parallel, thus, a single pass produces all the lumbers from the log. In contrast, band saws cut lumbers in a layer-bylayer fashion in each pass. This operational difference influences several parameters of these family of saws, that are relevant from the scheduling point of view. While each specific brand of equipment has their own specifications, in general, framesaws tend to be faster, cheaper to operate. However, the bands must be thicker resulting in more waste, and changing the cutting pattern requires non-negligible time. On the other hand, band saws can switch easily from one cutting pattern to another, moreover, if deficiencies in the log are detected (either by sensors or by experts operating the saw), agile decisions can be made mid-process to ensure quality products and minimize waste.

Another aspect often disregarded by literature models is the human resource requirement of the entire process, that has a wide range for the various equipment available. Highly automated modern equipment tends to require less human intervention from a highly trained employee. Facilities with large throughput and thus, revenue, tend to have less difficulty securing and training this smaller but specialized workforce. On the other hand, smaller facilities with older equipment require more workers for moving the logs, lumber and operating the saw. While the actual numbers depend on the specific unit, the difference between framesaws and bandsaws may also show in this segment, the former tending to require more people. The human-resource aspect highlights another issue that is more prevalent in smaller businesses: smaller production scale leads to less revenue, which implies smaller budget for investment, thus equipment is older and less modernized, requiring more employees with basic skillset. In the current workforce market, these companies with lower budget often have difficulty securing the additional operators needed for this older equipment. Shortage of such workforce is becoming a pressing issue for such companies.

The aim of this work is to provide an approach, that takes into account several of the aforementioned aspects of the sawmill industry, in order to better model its specific features, and provide more meaningful results. There are many productions specific details not yet addressed here, such as the maintenance frequency and cost, moisture content, and its effects, etc. The goal of this work is to make the first step in the direction of a very specific and detailed model, while evaluating the cost in complexity and computational time needed to solve it

The overall objective is to minimize cost associated with under-delivering for the accepted orders. The facility has both a framesaw and a bandsaw to utilize. Each equipment has its human resource requirement, and the employees are categorized into two groups: specialists, from whom at least one is needed for the operation of both equipment, and assistant workers – referred to workers later – for tasks like log and lumber movements, etc.

For each day of the planning horizon given are the available workers and specialists, the quantity in each lumber type to deliver. The facility has limited storage capacity for overproduction and there is a limited budget for daily hires as workers. Specialists may also substitute as workers if only one of the saws are operated.

The bandsaw may change cutting patterns any number of times during the shifts, however, framesaws are only allowed to do that once in a single shift. This limitation stems from industrial best practice. The cutting pattern of the framesaw may also be changed on its idle days.

Logs are presumed to be sorted into a finite number of classes, each having one or several cutting pattern, yielding predetermined ratio in a finite number of lumber types. Logs are presumed to be readily available and the beginning of the planning horizon, and of the same wood type.

The production planner has the flexibility to decide:

- On which days are additional hires employed.
- Which equipment is operated on each day.

- If the bandsaw is operated, how long each cutting pattern is used during the shift.
- If the framesaw is operated, what cutting pattern is used, and whether there is a change in the cutting pattern during the day. If so, when, and what is the new cutting pattern.
- The selection of the new cutting pattern if the framesaw is not operated.

III. PROPOSED MODEL

We propose a Mixed-Integer Linear Programming (MILP) model to provide the optimal short- or midterm schedule of the sawmill under investigation. The objective function can be summarized as follows:

$$\min \sum_{d \in \mathcal{D}} \sum_{t \in \mathcal{T}} LF_t \cdot u(p)_{d,t} \tag{1}$$

Where LF_t is the proportional late fee for lumber type t, and $u(p)_{d,t}$ is the underproduction for that lumber type on day d. Over- and underproduction for a day is managed by the following constraint:

$$y_{d,t} + o(p)_{d-1,t} - o(p)_{d,t} + u(p)_{d,t} \ge DM_{t,d}$$
$$\forall d \in \mathcal{D}, t \in \mathcal{T}$$
 (2)

Where $y_{d,t}$ denotes the daily production, $DM_{t,d}$ the delivery requirement. $o(p)_{d-1,t}$ is the overproduction from the previous day, that equals to the amount stored. Similarly, $o(p)_{d,t}$ represents the amount to be stored for the next day. This quantity is limited by overall storage capacity of the facility denoted by \mathcal{C} , and shared by all lumber types, as expressed in Equation (3):

$$\sum_{t \in \mathcal{T}} o(p)_{d,t} \le C \quad \forall d \in \mathcal{D}$$
 (3)

Daily production quantity is calculated based on Equation (4):

$$y_{d,t} = \sum_{p \in \mathcal{P}} Y_{t,p} \cdot V_{l_p} \cdot \left(q_{d,p}^{F,-} + q_{d,p}^{F,+} + q_{d,p}^B \right)$$

$$\forall d \in \mathcal{D}, t \in \mathcal{T}$$
(4)

Where V_{lp} indicates the volume of a log type l_p of the cutting pattern p, the parameter $Y_{t,p}$ expresses the ratio of the volume of lumber type t produced when using pattern p. Integer variables $q_{d,p}^{F,-}$, $q_{d,p}^{F,+}$, and $q_{d,p}^{B}$ indicate the number of logs cut by pattern p on day d by the frame saw before pattern change, after pattern change, and by the band saw respectively.

Naturally, the number of logs processed by both saws during the whole production horizon cannot exceed the stock available, denoted by I_l for each log type 1, as expressed in Equation (5):

$$\sum_{d \in \mathcal{D}} \sum_{\substack{p \in \mathcal{P} \\ l_n = l}} \left(q_{d,p}^{F,-} + q_{d,p}^{F,+} + q_{d,p}^{B} \right) \le I_l \quad \forall l \in \mathcal{L}$$
 (5)

The number of logs processed by the band saw is limited by the length of the shift H, and the sawing time ST_p^B for pattern p. Moreover, if the bandsaw is idle on day d, as indicated by a 0 value of the binary variable w_d^B , the overall production is zero.

$$\sum_{p \in \mathcal{P}} q_{d,p}^B \cdot ST_p^B \le H \cdot w_d^B \quad \forall d \in \mathcal{D}$$
 (6)

Modelling the specific behaviour of the framesaw requires several constraints:

$$\begin{aligned} q_{d,p}^{F,-} &\leq \frac{t_d}{ST_p^F} + \frac{H}{ST_p^F} \cdot \left(1 - s_{d,p}^{F,-}\right) \\ &\forall d \in \mathcal{D}, p \in \mathcal{P} \end{aligned} \tag{7}$$

$$q_{d,p}^{F,-} \leq \frac{H}{ST_{n}^{F}} \cdot s_{d,p}^{F,-} \quad \forall d \in \mathcal{D}, p \in \mathcal{P} \tag{8}$$

$$\begin{split} q_{d,p}^{F,+} &\leq \frac{H - t_d - CT^F \cdot \left(1 - s_{d,p}^{F,-}\right)}{ST_p^F} \\ &+ \frac{H}{ST_p^F} \cdot \left(1 - s_{d,p}^{F,+}\right) \quad \forall d \in \mathcal{D}, p \in \mathcal{P} \end{split} \tag{9}$$

$$q_{d,p}^{F,+} \leq \frac{H}{ST_{p}^{F}} \cdot s_{d,p}^{F,+} \quad \forall d \in \mathcal{D}, \, p \in \mathcal{P}$$
 (10)

In these constraints, continuous non-negative variable t_d indicates the time of changing the cutting pattern during the shift, if such an event occurs. Binary variables $s_{d,p}^{F,-}$ and $s_{d,p}^{F,+}$ indicate if pattern p is used before or after the change, respectively. Equations (7) and (8) express the relation $q_{d,p}^{F,-} \leq t_d \cdot \frac{s_{d,p}^{F,-}}{sT_p^F}$ in a linear form, where ST_p^F is the time needed to saw a log with pattern p on the framesaw. Equations (9) and (10) express the same relation after the change of the cutting pattern, excluding the changeover time for the new pattern, CT^F .

Similar to the bandsaw, if the framesaw is idle on day d, no logs can be processed by it, as expressed by Equations (11) and (12), where binary variable w_d^F indicates if the framesaw is operated on day d or not:

$$\sum_{p \in \mathcal{D}} s_{d,p}^{F,-} = w_d^F \quad \forall d \in \mathcal{D}$$
 (11)

$$\sum_{p \in \mathcal{P}} s_{d,p}^{F,+} = w_d^F \quad \forall d \in \mathcal{D}$$
 (12)

The persistence of the same cutting pattern on subsequent non-idle days is expressed by constraints (13) and (14):

$$s_{d,p}^{F,+} \ge s_{d+1,p}^{F,-} - 1 \cdot \left(2 - w_d^F - w_{d+1}^F\right) \\ \forall d \in \mathcal{D}, p \in \mathcal{P}$$
 (13)

$$s_{d,p}^{F,+} \le s_{d+1,p}^{F,-} + 1 \cdot \left(2 - w_d^F - w_{d+1}^F\right) \\ \forall d \in \mathcal{D}, p \in \mathcal{P}$$
 (14)

The following constraints address the human resource requirements posed by both sawmills:

$$RR^{SP,F} \cdot w_d^F + RR^{SP,B} \cdot w_d^B \le HR_d^{SP}$$

$$\forall d \in \mathcal{D}$$

$$(15)$$

$$RR^{AW,F} \cdot w_d^F + RR^{AW,B} \cdot w_d^B \le HR_d^{AW} + x_d + \left(HR_d^{SP} - RR^{SP,F} \cdot w_d^F - RR^{SP,B} \cdot w_d^B\right)$$

$$\forall d \in \mathcal{D}$$

$$(16)$$

Where integer parameters RR represent the number of workers (AW) and specialists (SP) for the framesaw (F) and bandsaw (B). Parameters HR_d^{SP} and HR_d^{AW} indicate the daily availability of specialists and workers, respectively. The nonnegative integer variable x_d denotes the number of additional hires for day d, who can only be employed in the role of workers, and Equation (16) also accounts for specialists substituting as workers.

Finally, the number of additional hires cannot exceed the predetermined number, as expressed in Equation (17):

$$\sum_{d \in \mathcal{D}} x_d \le X^{AW} \tag{17}$$

IV. EMPIRICAL RESULTS

The model proposed in Section III need to be investigated from two different aspects: practical applicability and efficiency. Thus, two different investigations are presented in this section. First, an example based on data from domain experts is investigated in more detail with special attention on the effect of workforce limitations. Second, computational performance is evaluated on a large number of randomly generated instances.

The implemented model was solved by Gurobi Optimizer 10.0.1 on a computer with an Apple M2 CPU and 16 GB of RAM available.

1. Practical investigation and preliminary efficiency tests

For the practical tests, 3 log sizes and 12 different lumber types were considered. The yield of the 5 cutting patterns were calculated with Pitago Optimizers [13] software. The time required to cut a single log on each machine for each cutting pattern was determined based on consultation with field experts, just as the changeover-time for the framesaw. The planning period was 1 week with a total number of 5 shifts of 8 hours. As stated before, both saws require one specialist, and for the scope of this study it was assumed that an additional worker

is needed for the bandsaw while 3 more is required for the framesaw. The availability of the employees for this study are given in **Table 1** for the planning horizon:

Table 1. Availability of employees

Day	Specialists	Assistant workers
1	2	1
2	2	1
3	1	3
4	2	1
5	1	3

The total demand was set for $366 m^3$, distributed among the days with $20 m^3$ of storage capacity. The lateness cost LF_t for each lumber was set homogeneously to $1 cu/m^3$, thus the objective is equivalent to minimizing undelivered quantity.

With no budget for additional hires the model was solved to optimality in 0.8328 seconds, and a schedule that could satisfy 38.19% of the demand. This schedule is shown on the first Gantt diagram in Fig. 3, and utilizes only the band saw, frequenting cutting patterns C and E.

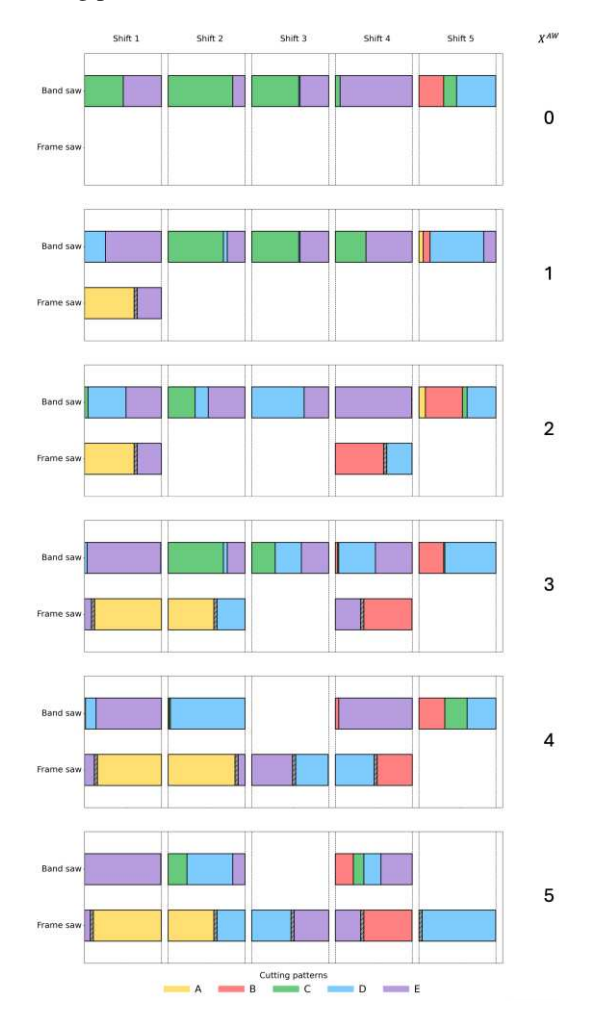


Figure 3. Gantt chart with 0 additional workers

In order to test the effect of potential additional hires, the model was solved repeatedly while incrementing the value of X^{AW} . As shown in **Fig. 4**, additional workers managed to increase the production to reduce the unmet demand. The first additional hire allowed the operation of the frame saw on the first shift, introducing cutting pattern A to the schedule, and reducing the unmet demand from by 17.29%. The introduction of a second additional hire reduced the optimum by a similar magnitude, 19.14%. This additional hire was utilized on the 4th shift, allowing the frame saw to operate on that day too. Interestingly, the prevalence of the cutting pattern C diminished, while B became favoured on both saws. The third addition provided a smaller effect of 13.07% and allowed the frame saw to operate on the second day too. The fourth additional hire shows the first schedule, where the band saw is idle on one of the days. The same change can be observed by allowing a 5th hire. In this schedule the frame saw is working every day, while the band saw is idle for 2 days. The unmet demand is reduced to 16.25%. The Gantt diagrams of the optimal schedules for each X^{AW} value can be seen in Fig. 3. Any further increase in the temporary workforce did not result in economic benefit. The sensitivity analysis on the diagram in Fig. 4 can be a valuable tool for the production planner to determine whether additional hires are worth investing into or not.

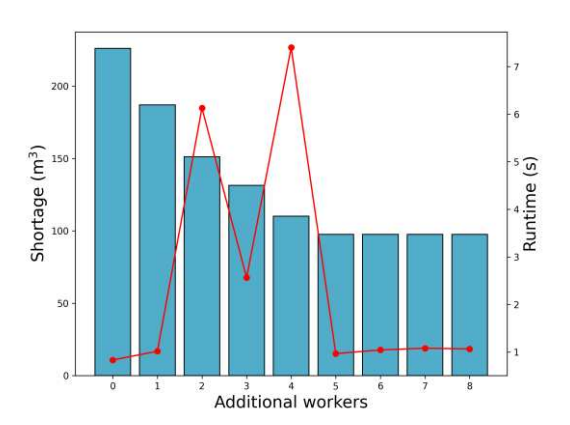


Figure 4. Result of additional worker increase

Fig. 4 also shows the CPU time needed to solve the model. It can be seen from the data, that the option for additional hires also increases the search space, thus the computational need as well. However, when no additional benefit can be gained by additional hires, no computational costs are paid for that flexibility either.

2. Computational tests on randomly generated examples

For a more extensive computational test, 6 groups of 50 examples were randomly generated and solved for planning periods ranging from 1 to 6 weeks. For

these 300 test cases, the technical parameters of the facility remained the same, and no additional hires were allowed. Within in each instance group corresponding to a planning period, the initial stock size and the cumulative demand of all lumber types were fixed, only the distribution of the demand and staff availability were altered. The stock size and cumulative demand was set proportional to the length of the corresponding planning period. For the instances of 1 week of planning period, 250 m^3 of initial stock of each log type and a total of 400 m^3 of demand was set.

In each test run, the time limit for the optimizer was set to 1500 seconds, which was only reached for outlier cases as shown on the box plot diagram with an exponential y scale in **Fig. 5**.

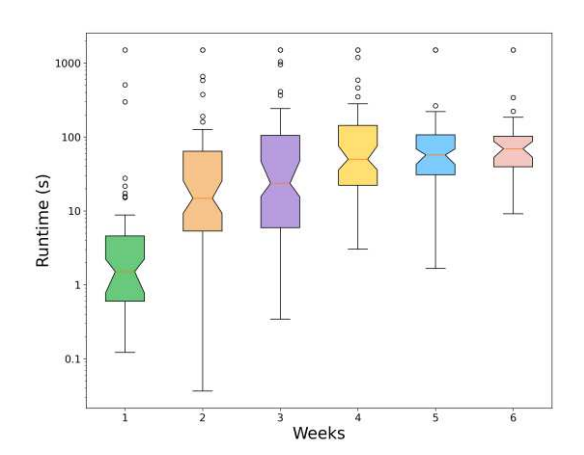


Figure 5. Computational need of solving the proposed model on randomly generated instances

The computational tests showed a surprising result. As the number of binary variables in the models increased linearly for each extension of the planning horizon, the required CPU time to solve the instances was expected to increase exponentially. This behaviour can be observed between the instance groups of 1 and 2 weeks of planning horizon. While later increases in the time horizon still resulted in larger CPU times, the change is less drastic, and by week 5 this seems to flatten out. Much larger examples for long-term planning would probably still become unsolvable in a reasonable amount of time. However, practical significance of short- and mid-term planning is much higher, thus these tests focused on planning periods up to one and a half months, where the proposed model proved to be applicable. This also means, that there is potential room to include further practical details while keeping computational needs on a reasonable level.

REFERENCES

[1] A. Santos, A. Carvalho, A. P. Barbosa-Póvoa, A. Marques, and P. Amorim, "Assessment and optimization of sustainable

V. CONCLUDING REMARKS

We developed a MILP formulation for the scheduling of smaller sawmills whose novelty lies in addressing several domain specific features of this production process, such as the different parameters of framesaws and bandsaws, and the workforce challenges facing the industry. The aim of integrating these features into the mathematical model responsible for production planning was to provide solutions that adhere to these practical considerations instead of risking sub-optimality by adjusting the schedule in a later phase of the decision-making process. The sensitivity analysis on the workforce availability showed the significance of these parameters on the optimal schedule, underlining the importance of its integration. The computational efficiency of the model has been tested on numerous examples and proved to be a suitable tool for short- and mid-term problems, that enables further research towards more detailed and complex models.

ACKNOWLEDGEMENT

The publishing of this paper was supported by the ÚNKP-23-1-I-SOE-127 New National Excellence Program of the Ministry for Culture and Innovation from source of the National Research, Development and Innovation Fund. The authors would also like to thank researchers in timber engineering from University of Sopron and InnoRenew CoE for their consultations.

AUTHOR CONTRIBUTIONS

Csaba Kebelei: Problem definition, model implementation, testing, writing, editing.

Mate Hegyhati: Problem definition, model development, writing.

DISCLOSURE STATEMENT

The authors declare that they have no known competing financial interests or personal relationships that could have appeared to influence the work reported in this paper.

ORCID

Cs. Kebelei <u>https://orcid.org/0009-0007-1132-638X</u>

M. Hegyhati https://orcid.org/0000-0003-3689-9866

forest wood supply chains — A systematic literature review," *Forest Policy and Economics*, vol. 105. 2019. https://doi.org/10.1016/j.forpol.2019.05.026

- [2] M. A. Hoogstra-Klein and K. Meijboom, "A qualitative exploration of the wood product supply chain investigating the possibilities and desirability of an increased demand orientation," For Policy Econ, vol. 133, 2021.
 https://doi.org/10.1016/j.forpol.2021.10260
- [3] N. Kazemi, N. M. Modak, and K. Govindan, "A review of reverse logistics and closed loop supply chain management studies published in IJPR: a bibliometric and content analysis," *International Journal of Production Research*, vol. 57, no. 15–16. 2019. https://doi.org/10.1080/00207543.2018.147 1244
- [4] S. Koch, S. König, and G. Wäscher, "Integer linear programming for a cutting problem in the wood-processing industry: A case study," *International Transactions in Operational Research*, vol. 16, no. 6, 2009. https://doi.org/10.1111/j.1475-3995.2009.00704.x
- [5] S. Maturana, E. Pizani, and J. Vera, "Scheduling production for a sawmill: A comparison of a mathematical model versus a heuristic," *Comput Ind Eng*, vol. 59, no. 4, 2010.

 https://doi.org/10.1016/j.cie.2010.07.016
- [6] N. Vanzetti, D. Broz, G. Corsano, and J. M. Montagna, "An optimization approach for multiperiod production planning in a sawmill," For Policy Econ, vol. 97, 2018. https://doi.org/10.1016/j.forpol.2018.09.001
- [7] D. Broz, N. Vanzetti, G. Corsano, and J. M. Montagna, "Goal programming application for the decision support in the daily

- production planning of sawmills," *For Policy Econ*, vol. 102, 2019. https://doi.org/10.1016/j.forpol.2019.02.004
- [8] P. P. Alvarez and J. R. Vera, "Application of Robust Optimization to the Sawmill Planning Problem," *Ann Oper Res*, vol. 219, no. 1, 2014. https://doi.org/10.1007/s10479-011-1002-4
- [9] M. Varas, S. Maturana, R. Pascual, I. Vargas, and J. Vera, "Scheduling production for a sawmill: A robust optimization approach," *Int J Prod Econ*, vol. 150, 2014. https://doi.org/10.1016/j.ijpe.2013.11.028
- [10] M. Kazemi Zanjani, D. Ait-Kadi, and M. Nourelfath, "Robust production planning in a manufacturing environment with random yield: A case in sawmill production planning," *Eur J Oper Res*, vol. 201, no. 3, 2010. https://doi.org/10.1016/j.ejor.2009.03.041
- [11] M. Morin *et al.*, "Machine learning-based models of sawmills for better wood allocation planning," *Int J Prod Econ*, vol. 222, 2020. https://doi.org/10.1016/j.ijpe.2019.09.029
- [12] V. Nasir, J. Cool, and F. Sassani, "Acoustic emission monitoring of sawing process: artificial intelligence approach for optimal sensory feature selection," *International Journal of Advanced Manufacturing Technology*, vol. 102, no. 9–12, 2019. https://doi.org/10.1007/s00170-019-03526-3
- [13] Pitago Optimizers. Available: https://pitago.eu/. Accessed: 2024-05-03.



This article is an open access article distributed under the terms and conditions of the Creative Commons Attribution NonCommercial (CC BY-NC 4.0) license.

AJ

ACTA TECHNICA JAURINENSIS

Vol. 17, No. 3, pp. 111-117, 2024 10.14513/actatechjaur.00742



Research Article

Optimise Energy Consumption of Wireless Sensor Networks by using modified Ant Colony Optimization

Yasameen Sajid Razooqi^{1,2,3,*}, Muntasir Al-Asfoor^{2,4}, Mohammed Hamzah Abed^{2,5}

 Al-Qadisiyah Education Directorate, 58002 Al Diwaneyah, Iraq
 Computer Science Department, Al Qadidiyah University, 58002 Al Diwaneyah, Iraq
 Department of Networked Systems and Services, Budapest University of Technology and Economics, Magyar tudósok körútja 2, 1117 Budapest, Hungary

⁴ Buckinghamshire New University, Queen Alexandra Rd, High Wycombe HP11, UK
 ⁵ Department of Telecommunications and Media Informatics, Budapest University of Technology and Economics, Magyar tudósok körútja 2, 1117 Budapest, Hungary
 *e-mail: yasameen.sajid@qu.edu.iq

Abstract:

Routing represents a pivotal concern in the context of Wireless Sensor Networks (WSN) owing to its divergence from traditional network routing paradigms. The inherent dynamism of the WSN environment, coupled with the scarcity of available resources, engenders considerable challenges for industry and academia alike in devising efficient routing strategies. Addressing these challenges, a viable recourse is applying heuristic search methodologies to ascertain the best path in WSNs. Ant Colony Optimization (ACO) is a well-established heuristic algorithm that has demonstrated notable advancements in routing contexts. This paper presents an altered routing protocol that is based on ant colony optimization. In this protocol, we incorporate the inverse of the distance between nodes and their neighbours in the probability equations of ACO, along with considering pheromone levels and residual energy. These formulation modifications facilitate the selection of the most suitable candidate for the subsequent hop, effectively minimising the average energy consumption across all nodes in each iteration. Furthermore, in this protocol, we iteratively fine-tune ACO's parameter values based on the outcomes of several experimental trials. The experimental analysis is conducted through a diverse set of network topologies, and the results are compared against well-established ACO algorithms and routing protocols. The efficacy of the proposed protocol is assessed based on various performance metrics, encompassing throughput, energy consumption, network lifetime, energy consumption, the extent of data transferred over the network, and the length of paths traversed by packets. These metrics collectively provide a comprehensive evaluation of the performance attainments of the routing protocols.

Keywords: WSN; Energy consumption; Optimization; ACO

I. INTRODUCTION

Wireless Sensor Networks (WSNs) encompass a set of miniature sensors designed to gather data from the observed environment and transmit it to a central base station known as the Sink [1]. Based on the specific application or purpose, these sensors can collect diverse data types, including temperature, noise, and pressure. The Sink processes the received data and may forward it to remote users or cloud platforms, facilitating integration with the Internet of Things (IoT). The IoT finds extensive applications in various domains, such as forest and ocean monitoring, nuclear reactor area management, and healthcare [2]. **Fig. 1** depicts the integration of WSN with IoT. Each sensor comprises three principal

components: the sensing unit responsible for data acquisition, the processing unit housing storage memory, and the communication unit for data transmission and reception. Additional elements, such as GPS and mobilisers for mobility management in the case of mobile sensors, may also be incorporated, albeit at the expense of higher energy consumption [3]. Solar cells can be integrated as an auxiliary power source to address energy constraints [4]. However, the primary power source for sensors remains batteries, posing a significant challenge in WSNs, as these batteries are typically non-rechargeable and non-replaceable due to the sensors' remote and hazardous deployment locations, their small size and low cost [5]. The communication phase incurs the highest energy

consumption, surpassing that of sensing and processing. Given the extensive deployment of sensors over vast geographical areas, manual management becomes impractical, necessitating dynamic routing techniques in WSNs to minimize energy consumption during communication. Achieving this objective involves leveraging artificial intelligence techniques and distributed algorithms to learn the network topology and determine energy-efficient paths [6][7]. This study proposes enhancing flat routing protocols for WSNs by modifying the traditional ACO algorithm.

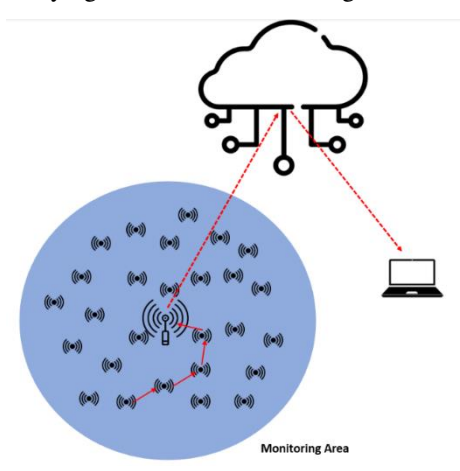


Figure 1. Wireless Sensor Network components and their integration with IoT [4]

Routing in Wireless Sensor Networks (WSNs) presents several formidable challenges, including those about energy consumption, communication range, and the establishment of peer-to-peer (P2P) communications. In P2P networks, all devices are interconnected with equal permissions and shared responsibilities for data processing. Unlike client and server networks, no specific devices in P2P networks are designated solely for sending or receiving data [8]. Each device possesses the same rights as its peers and can fulfil analogous functions. Consequently, in WSNs, each sensor must judiciously select the most suitable neighbour within its communication range, facilitating the formation of efficient multi-hop paths leading to the sink node. The goal is to minimize the distance traversed and, thus, conserve energy during data transmission. Fig. 2 visually depicts the sensing and communication ranges of the sensors.

Routing in Wireless Sensor Networks (WSNs) determines network lifetime and performance. Given the reliance of sensors on battery power and the significant consumption in communication, efficient routing management is essential to reduce energy consumption while maintaining high throughput. This study proposes leveraging Artificial Intelligence (AI) algorithms to determine the next hop or candidate neighbour for packet transmission,

a key distinction of WSN routing from other network types. Each sensor possesses limited knowledge of its immediate neighbours within its communication range rather than the entire network, necessitating novel approaches for flat routing protocols that do not rely on central nodes. In order to tackle this problem, we are presenting smart routing protocols. This protocol uses a modified (ACO) algorithm to select the next node while searching for the sink (destination). The modification involves performing thorough testing and analysis of various network topologies to determine the optimal parameter values $(\alpha, \beta, \rho, \gamma, \text{ and } Q)$ for ACO in the flat routing protocol within WSNs. To mitigate energy consumption, propose reducing we communication range of the sensors to prevent packets from being transmitted across long distances, a strategy based on the energy model discussed later. Additionally, we aim to minimise the Time-to-Live (TTL) value (number of hops) based on the network size. Furthermore, to address the issue of fast node depletion in flat protocols, we propose using super sensors near the sink to handle high loads efficiently, mitigating the risk of nodes dying prematurely. These suggested strategies are expected to improve the efficiency and performance of flat routing protocols in WSNs, leading to prolonged network lifetime and enhanced overall operation.

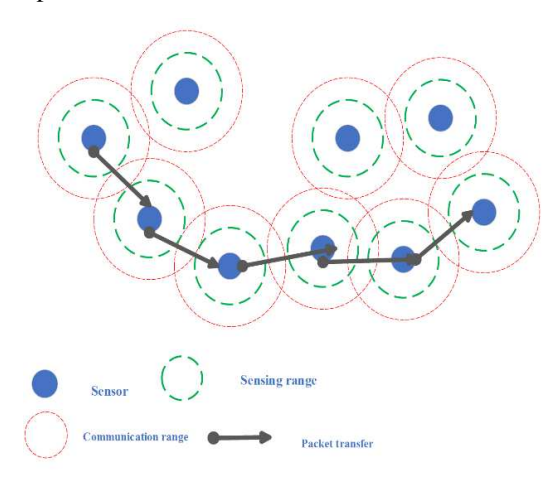


Figure 2. Shows the packet routing in WSN based on the communication range

This paper is organised as follows: Section Two presents the related work, and Section Three presents the materials and proposed models of this work, followed by a result analysis illustrated in Section Four. Section five concludes all the concepts and the future direction in this research field.

II. RELATED WORK

This section reviews various research studies focused on reducing energy consumption in Wireless Sensor Networks (WSN) through hierarchical and flat routing approaches. In one study [8], the

researchers employed Capsule Neural Network to develop a learning model for identifying suitable cluster heads within the cluster based on identity records. They also utilized shortest path selection to identify forward nodes outside the clusters, reducing energy consumption. In another research effort [9], gravitational force and fuzzy rules were integrated to construct clusters and manage routing, improving network lifetime. Where the fuzzy logic has been used to select appropriate nodes as cluster heads, on the other hand, the Energy-efficient Scalable Clustering Protocol [10] addressed distances and within clusters to generate between equiponderant clusters. The Particle Swarm Optimization technology based on Dragonfly's algorithm (DA-PSO) was employed to select a cluster head, along with a new energy-efficient fitness function for optimal CH selection. However, hierarchical routing protocols suffer inefficiencies in cluster head selection and frequent cluster head changes during the network's lifetime, along with the rapid depletion of cluster heads due to their dual roles of collecting sensing data and forwarding it to the sink.

In another study [11], the researcher proposed an intelligent opportunistic routing protocol (IOP) using a machine learning technique to select the next hop based on residual energy.

It is important to note that the heuristic function based solely on save the residual energy in [12][13] did not guarantee to reach the sink in fewer hops, resulting in decreased throughput despite high energy consumption. One significant limitation of flat routing protocols is the rapid energy depletion of sensors near the sink due to the heavy load of transmitting sensing data from other sensors. In contrast, the proposed protocol addresses this limitation by utilizing solar cells as a power supply for the sensors near the sink and leveraging methods based on artificial intelligence to find the minimum length of the success path, thereby enhancing energy efficiency.

III. MATERIALS AND METHODS

1. Network setting

Two distinct models govern the distribution of sensors within the monitoring area: the pre-planned mode, wherein the monitoring area is readily accessible for manual sensor deployment and management, resulting in efficient coverage with a reduced number of sensors, and the ad-hoc mode, which assumes greater significance in challenging or distant environments where manual access is impractical. In the ad-hoc mode, a larger number of sensors are deployed randomly to achieve the required coverage [14][15][16]. The latter distribution model was adopted during the network's construction phase, randomly deploying N sensors

within a square area. The network configurations encompassed three setups, each varying in the number of nodes and network area: 80 nodes in a 100x100-meter region, 160 nodes in a 200x200-meter region, and 240 nodes in a 300x300-meter region.

During the network operation, each sensor initiates communication by sending a hello packet to its sensors. neighbouring conveying essential information such as ID, location, and energy status. Data transfer within the network was categorized into three modes: event-driven, where data transmission commences upon specific events; timedriven, wherein sensed data is transmitted to the sink at predetermined intervals; and query-driven, where data transmission is triggered in response to sensor requests [6]. In the proposed model, the first type, i.e., event-driven data transfer, was adopted to enable a specific group of sensors to transmit their sensing data during each operational round. To simulate this behaviour, the set of sensors responsible for data transmission during each round was randomly selected.

2. Energy model

This study assumes that all sensors initially possess equal energy levels. However, over time, each sensor's energy varies due to energy depletion during the sensor operations (sensing, data processing, and communication). The energy expended on sensing and processing is minimal compared to the energy used for communication [17].

Every sensor keeps an information table about neighbouring nodes: their IDs, remaining energy levels, and positions. The Euclidean distance formula calculates the distance between nodes, and any changes in energy levels are promptly updated in the table. We utilize the equations specified in reference [18] to evaluate energy consumption during communication. Specifically, one of two equations is applied depending on the distance between sender and receiver sensors. When the distance is below a predefined threshold "d0," the free space model is employed. On the other hand, if the distance surpasses this threshold, the multipath fading model calculates the energy needed for transmitting a 1-bit packet.

$$E_T(l,d) = \begin{cases} lE_{elec} + \varepsilon_{fs}d^2 & if \ d < d_o \\ lE_{elec} + \varepsilon_{mp}d^4 & if \ d \ge d_o \end{cases}$$
 (1)

where E_{elec} is the energy of the electronic circuit, while \mathcal{E}_{fs} and \mathcal{E}_{mp} are the energy consumed. In the receiver sensor, energy lost in receiving l bits is:

$$ER(l) = lE_{elec} \tag{2}$$

3. Ant colony optimization

Ant Colony Optimization (ACO) Wireless Sensor Networks (WSNs) use pheromone information to help sensor nodes select suitable neighbors. In this study, we propose enhancement of Ant Colony Optimization for flat routing protocol, an intelligent protocol based on ACO. Initially, all connections between sensors are assigned uniform initial pheromone values. Consequently, during the first hop, sensor nodes make their next-hop selections without being influenced by pheromone concentration. However, the pheromone values are updated with each successive round, impacting the subsequent next-hop selections.

To enhance the heuristic function in the probability equation, we suggest two methods in the proposed Modified ACO. Firstly, we employ the inverse of the distance between nodes i and j to establish the heuristic function η_{ij} , favouring a higher probability for shorter distances, thereby encouraging the selection of closer sensors. Secondly, we incorporate two additional heuristic functions, along with the pheromone value, by incorporating the distance between nodes i and j and the residual energy of the neighbour sensor. Consequently, the probability equation takes the form of equation (3):

$$parentp_{ij}^{m}(t) = \frac{\left[\tau_{ij}(t)\right]^{\alpha} \cdot \left[n_{ij}(t)\right]^{\beta}}{\sum_{m \in N_{i}^{k}} \left[\tau_{im}(t)\right]^{\alpha} \cdot \left[n_{im}(t)\right]^{\beta}},$$

$$if \ j \in N_{i}^{k}$$
(3)

where η_{ij} represents the inverse of the distance between nodes i and j, and δ_j denotes the difference between the initial and residual energy of node j.

To perform pheromone updates, we utilized equations 4 and 5.

$$\tau_{ij}(t + \Delta t) = (1 - \rho).\tau_{ij}(t) \tag{4}$$

for all edge in the network, and

$$\tau_{ij}(t + \Delta t) = \tau_{ij}(t) + \Delta \tau_{ij}(t) \tag{5}$$

for all success paths.

The ACO's parameters (α , β , ρ , γ , and Q) were systematically adjusted after conducting rigorous testing and analysis across the three network topologies to determine the values that optimise high throughput while minimising energy consumption, rendering ACO suitable for this particular context. Algorithm 1 illustrates the modified ACO algorithm. Ant Colony Optimization 1 and 2 focus on minimum distance and energy, respectively.

IV. EXPERIMENT RESULT AND ANALYSIS

This section provides a comprehensive overview of the networks' attributes, the simulation environment employed, the designated parameters, and the performance evaluation results for the two proposed protocols. Additionally, we present a comparative analysis of the outcomes of these protocols concerning the performance metrics adopted for the evaluation. Furthermore, we juxtapose the results of the proposed protocols against other algorithms, which are utilities in flat routing approaches used in Wireless Sensor Networks (WSNs).

1. Environment simulations

In the simulation of network configuration, implementation of routing protocols, and subsequent result analysis, we utilised the Python programming language, complemented by the NetworkX package. To substantiate the efficacy of our proposed protocols, we conducted simulations on three distinct networks. These networks comprised 80 nodes in a 100x100-meter area, 160 nodes in a 200x200-meter area, and 240 nodes in a 300x300-meter area. **Table 1** shows the network scenarios in our experiment, parameters of the network's scenarios.

Table 1. Network scenarios

Parameters	Scenario 1	Scenario 2	Scenario 3
Network Area	100x100 m ²	200x200 m ²	300x300 m ²
Base station location	(50,50)	(100,100)	(150,150)
Number of sensors	80	160	240
Deployment	Random scale free	Random scale free	Random scale free
Communica tion range	20 m	28 m	35 m

Furthermore, **Table 2** accounts for the parameters employed in the network model, energy model, and the Ant Colony Optimization (ACO) algorithm. We maintained consistent parameters throughout our experimental analysis for all the cases.

Table 2. Experimental parameters

Parameters	Value
Initial energy of sensors	5 J
Number of sinks	1
Location of sink	Centre of area
Packet size	1024
Eelec	50 nJ/bit
\mathcal{E}_{mp}	0.0013 pJ/bit/m4
\mathcal{E}_{fs}	10 pJ/bit/m2
d_0	50
α	2
β	3
Initial pheromone	1
ρ	0.5 - 1
Q	1

2. Result and analysis

This study comprehensively assessed the simulation outcomes encompassing throughput, energy consumption, network lifetime, and success message ratio travelled by data packets. We have juxtaposed the performance of our proposed ACObased routing algorithm, outlined in [16], with that of the conventional ACO routing protocol under identical simulation conditions, thus substantiating the efficacy of the algorithms in question. In the subsequent section, we will expose each of the metrics above, delineated to two distinct scales: the count of network operation iterations or rounds and the progressive Time-to-Live (TTL) range. Each TTL value corresponds to the network's performance following 1000 iterations of network operation. Furthermore, these metrics will be illustrated across three distinct network topologies, explained in Table

The throughput metric indicates the successful delivery of packets to their intended destinations, with the success ratio employed as an illustrative measure in our calculations. The figures presented above conspicuously demonstrate the notable superiority of the ACO-based routing protocol (Table 3) in achieving elevated throughput compared to both the traditional ACO protocol and energy and randomness-based routing approaches. Fig. 3 and 4 visually depict the success rates across the three network topologies during operational iterations varving and energy consumption. Additionally, Fig. 5 showcases the metrics as mentioned above in scenarios involving different TTL values, thereby further substantiating the superior throughput performance of our proposed ACO-based routing protocol. Fig. 6 shows a final comparison of the Network's lifetime among three scenarios, which is explained in Table 1. And it shows the proposed ACO achieved high performance compared to the traditional methods.

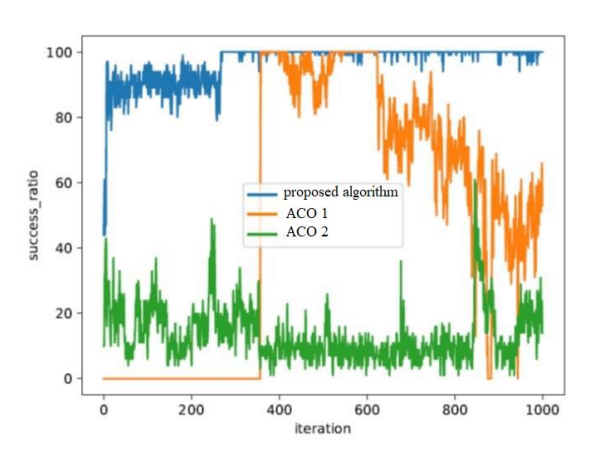


Figure 3. Success message ratio based on 160 network nodes.

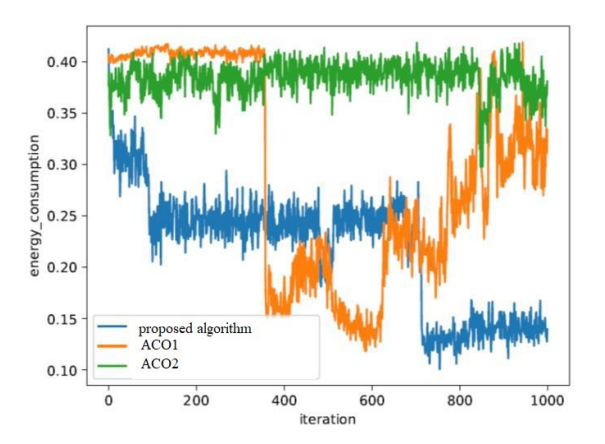


Figure 4. Energy consumption ratio based on 160 network nodes.

Table 3. ACO-based routing protocol algorithm

Input: Energy nodes: 5 j Set No of hops Energy: electronic circuit, amplifier in free space , amplifier in multi path Set L: Packet size Output: Successful path Steps: Received energy= L* electronic circuit While no of hops!=0 do:

Sort the neighbors based on distance and maximum ACO probability using Eq(3)

Create node list to visit

If no of hops ==0 then:

Return (fail)

Else:

Visit the nodes list

Update the success path

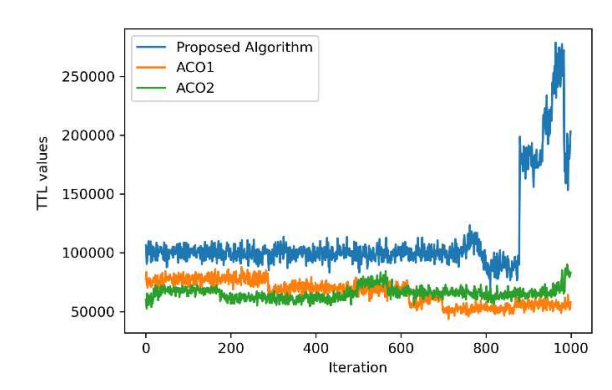


Figure 5. TTL values over 160 network nodes

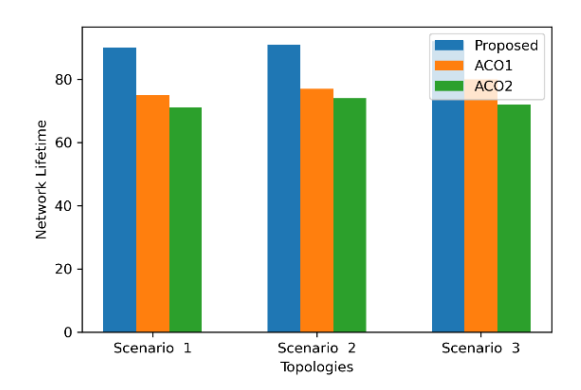


Figure 6. Comparison of Network's lifetime for three models and three scenarios

V. CONCLUSION

In this research endeavour, we present a series of intelligent routing protocols designed to enhance the operational longevity of Wireless Sensor Networks (WSNs). Our primary objective revolves around the optimisation of energy utilisation within these networks. To achieve this, we leverage the heuristic search optimisation approach known as Ant Colony Optimization (ACO). Our efforts encompass refining the underlying pheromone concentration equations within the ACO algorithm. Moreover, we meticulously fine-tune the pivotal ACO parameters $(\alpha, \beta, \rho, \gamma, \text{ and } Q)$ based on an iterative process involving comprehensive testing across diverse network topologies. This meticulous parameter calibration is geared towards rendering the ACO algorithm conducive to seamless integration within the framework of flat routing protocols within WSNs. The proposed algorithm's efficacy is examined across three distinct yet controlled network scenarios. These scenarios encapsulate 80 nodes deployed within a 100x100 meter area, 160 nodes spanning a 200x200 meter expanse, and 240 nodes dispersed across a 300x300 meter terrain.

REFERENCES

- [1] M.M. Kumar; A. Chaparala. OBC-WOA: opposition-based chaotic whale optimization algorithm for energy efficient clustering in wireless sensor network. Intelligence 12 (6) (2019) pp. 249-258.
 - https://doi.org/10.22266/ijies2019.1231.24
- [2] K. Bajaj, B. Sharma, and R. Singh: Integration of WSN with iot applications: A vision, architecture, and future challenges, in EAI/Springer Innovations in Communication and Computing, 2020. https://doi.org/10.1007/978-3-030-38516-3 5
- [3] T. K. Jain, D. S. Saini, and S. V. Bhooshan: Lifetime optimization of a multiple sink wireless sensor network through energy balancing, Journal of Sensors 2015 (2015) 21250.

Notably, all evaluated scenarios are governed by identical network and energy parameters, ensuring an equitable basis for comparison. The evaluation outcomes compellingly underscore the superior performance of the proposed modified ACO algorithm. This superiority contrasts not only with the conventional ACO algorithm, as documented in [16], but also against a spectrum of alternative protocols. This performance is consistently evident across all dimensions of performance metrics embraced within this comprehensive study.

ACKNOWLEDGEMENT

We would like to thank Al-Qadisiyah University, Buckinghamshire New University, and Budapest University of Technology and Economics for their support.

AUTHOR CONTRIBUTIONS

Y.Razooqi: Conceptualization, Experiments, Theoretical analysis.

Al-Asfoor: Supervision, Review and editing.

M.Abed: Supervision, Review and editing.

DISCLOSURE STATEMENT

The authors declare that they have no known competing financial interests or personal relationships that could have appeared to influence the work reported in this paper.

ORCID

Y.Razooqi https://orcid.org/0000-0003-2315-067X
Al-Asfoor https://orcid.org/0000-0003-4780-4252
M.Abed https://orcid.org/0000-0003-4780-4252

https://doi.org/10.1155/2015/921250

- [4] V. Sharma and A. Pughat: Introduction to energy-efficient wireless sensor networks, in Energy-Efficient Wireless Sensor Networks, 2017.
 - https://doi.org/10.1201/9781315155470
- [5] B. Rashid and M. H. Rehmani: Applications of wireless sensor networks for urban areas: A survey, Journal of Network and Computer Applications 60 (2016) pp. 192-219. https://doi.org/10.1016/j.jnca.2015.09.008
- [6] R. E. Mohamed, A. I. Saleh, M. Abdelrazzak, and A. S. Samra: Survey on Wireless Sensor Network Applications and Energy Efficient Routing Protocols, Wireless Personal Communications 101 (29) (2018) pp. 1019-1055.

https://doi.org/10.1007/s11277-018-5747-9

- [7] M. Elshrkawey, S. M. Elsherif, and M. Elsayed Wahed: An Enhancement Approach for Reducing the Energy Consumption in Wireless Sensor Networks, J. King Saud Univ. -Comput. Inf. Sci. 30 (2) (2018) pp. 259-267. https://doi.org/10.1016/j.jksuci.2017.04.002
- [8] Razooqi, Yasameen Sajid, and Muntasir Al-Asfoor: Intelligent routing to enhance energy consumption in wireless sensor network: a survey. in Mobile Computing and Sustainable Informatics: Proceedings of ICMCSI 2021. Springer (2021) pp. 283-300. https://doi.org/10.1007/978-981-16-1866-6 21
- [9] M. Selvi, S. V. N. Santhosh Kumar, S. Ganapathy, A. Ayyanar, H. Khanna Nehemiah, and A. Kannan: An Energy Efficient Clustered Gravitational and Fuzzy Based Routing Algorithm in WSNs, Wirel. Pers. Commun. 116 (1) (2021) pp. 61-90. https://doi.org/10.1007/s11277-020-07705-4
- [10] H. Singh and D. Singh: An Energy Efficient Scalable Clustering Protocol for Dynamic Wireless Sensor Networks, Wirel. Pers. Commun. 109 (4) (2019) pp. 2637-2662. https://doi.org/10.1007/s11277-019-06701-7
- [11] D. K. Bangotra, Y. Singh, A. Selwal, N. Kumar, P. K. Singh, and W. C. Hong: An intelligent opportunistic routing algorithm for wireless sensor networks and its application towards e-healthcare, Sensors 20 (14) (2020) 3887.

https://doi.org/10.3390/s20143887

[12] A. El Ghazi, B. Ahiod, and A. Ouaarab: Improved ant colony optimization routing protocol for wireless sensor networks, in Lecture Notes in Computer Science 2014, vol. 8593 LNCS. https://doi.org/10.1007/978-3-319-09581-3 17

[13] J. Zhang: Real-time detection of energy consumption of IoT network nodes based on artificial intelligence, Comput. Commun. 153 (2020) pp. 188-195. https://doi.org/10.1016/j.comcom.2020.02.015

[14] Z. Al Aghbari, A. M. Khedr, W. Osamy, I. Arif, and D. P. Agrawal: Routing in Wireless Sensor Networks Using Optimization Techniques: A Survey, Wirel. Pers. Commun. 111 (4) (2020) pp. 2407-2434. https://doi.org/10.1007/s11277-019-06993-9

- [15] Razooqi, Yasameen Sajid, and Muntasir Al-Asfoor: Energy Aware Nature inspired Routing for Wireless Sensor Networks. 2021 7th International Conference on Contemporary Information Technology and Mathematics (ICCITM). IEEE, 2021. https://doi.org/10.1109/ICCITM53167.2021.9677837
- [16] Razooqi, Yasameen Sajid, and Muntasir Al-Asfoor: Enhanced Ant Colony Optimization for Routing in WSNs An Energy Aware Approach. International Journal of Intelligent Engineering & Systems 14 (6) (2021) pp. 442-452.

https://doi.org/10.22266/ijies2021.1231.39

- [17] Al-Asfoor, Muntasir, and Mohammed Hamzah Abed: The effect of the topology adaptation on search performance in overlay network. Expert Clouds and Applications: Proceedings of ICOECA 2021. Springer Singapore pp, 65-73. https://doi.org/10.1007/978-981-16-2126-0_7
- [18] S. Yousefi, F. Derakhshan, H. Karimipour, and H. S. Aghdasi: An efficient route planning model for mobile agents on the internet of things using Markov decision process, Ad Hoc Networks 98 (2020) 102053. https://doi.org/10.1016/j.adhoc.2019.102053



This article is an open access article distributed under the terms and conditions of the Creative Commons Attribution NonCommercial (CC BY-NC 4.0) license.



ACTA TECHNICA JAURINENSIS

Vol. 17, No. 3, pp. 118-129, 2024 10.14513/actatechjaur.00749



Research Article

Reducing Energy Demand in Concrete Pavements by the Use of Blended Cements

Réka Szpotowicz¹ and Csaba Tóth^{1,*}

Department of Highway and Railway Engineering, Budapest University of Technology and Economics, Müegyetem rkp. 3., K épület magasföldszint 98., 1111 Budapest, Hungary *e-mail: toth.csaba@emk.bme.hu

Abstract:

This research explores strategies to minimise energy consumption and enhance environmental sustainability in road construction. Focusing on concrete pavement structures, the study evaluates the impact of substituting Portland cement with environmentally friendly alternatives such as fly ash and blast furnace slag. A comprehensive model is employed to analyse the energy demands of different pavement types, considering various cement replacements over their lifetime, from the initial extraction of materials to the conclusion of construction. Results indicate an energy saving potential of 8.63% by substituting 10% of Portland cement with fly ash, while an impressive reduction of 58.63% in cement production energy is achieved by replacing Portland cement with 80% blast furnace slag. The study underscores the significant role of cement variations in mitigating energy consumption, emphasizes the potential of blast furnace slag as a sustainable alternative as well as highlights the significance of alternative cement types in reducing energy consumption in concrete pavement construction, aligning with environmental sustainability goals and offering insights for more eco-friendly infrastructure development.

Keywords: Sustainability; Blended cements; Concrete structures; Energy; Reduction of energy consumption

I. INTRODUCTION

The energy and climate crises call for urgent action by decision-makers, road project investors, and others. The European Parliament and the Council made significant strides toward achieving carbon neutrality in Europe by ratifying the Climate Change Act in 2021, elevating the EU's interim emissions reduction target for 2030 from 40% to a minimum of 55%. "Fit for 55" includes emissions regulations and decarbonisation efforts in various sectors, including road management, targeting the concrete and asphalt industries to reduce emissions and energy consumption.

AzariJafari et al. [1] found that achieving carbonneutral pavements by 2050 is only feasible with policy and industry interventions. Without decarbonization efforts, US road construction material emissions could increase by 19.5% by 2050. Transitioning to renewable energy sources for road materials is crucial for meeting decarbonization goals.

Understanding the anticipated energy demand throughout each infrastructure layer's production,

construction, and operational phases is vital for making informed construction and renewal decisions. Implementing an efficient management system, as proposed by Volkov et al. [2], could further optimize the energy demand in concrete pavement projects by streamlining resource allocation and operational processes. Concrete pavements offer greenhouse gas savings and longevity, reducing maintenance and improving fuel efficiency. They also have a cooling effect and contribute to carbon dioxide removal [3]. A previous study conducted in Hungary investigated the energy consumption of various construction processes [4]. The findings revealed that concrete pavements had, on average, 60% higher energy demand than asphalt structures in the examined pavement types. This notable disparity predominantly stemmed from utilizing high-energy-demand Portland cement (CEM I). In this article, we extend this research by exploring the potential reduction in the modelled energy demand of these Hungarian concrete pavements by adopting environmentally friendly cement types.

II. STRATEGIES TO REDUCE ENERGY DEMAND IN CEMENT PRODUCTION

According to CEMBRUREU (The European Cement Association), the total cement production for 2020 reached 4.17 billion tonnes.

The breakdown is as follows [5] (Mt means a million tonnes):

China: 2377 Mt;
India: 290 Mt;
EU27: 171.5 Mt;
USA: 89 Mt.

The carbon dioxide emissions averaged 783 kg CO₂/tonne of cement in 1990. The Association aims to cut CO₂ emissions from cement production to 472 kg CO₂/tonne by 2030 and achieve carbon neutrality by 2050, which aligns with the Paris Agreement. The report outlines the potential for reducing CO₂ emissions during clinker, cement, concrete production, construction, and (re)carbonation. Implementing the following measures plays a significant role in achieving emission reductions: technological investments, policy adjustments, and production changes throughout the life cycle, spanning from production and clinker production to concrete recarbonation and recycling [6-11]. For instance:

- incorporating alternative fuels like nonrecyclable waste and biomass-derived sources to substitute fossil fuels;
- implementing more energy-efficient furnaces;
- advancing the utilization of innovative, lowclinker concrete;
- introducing and enhancing carbon capture and storage/utilization technologies (CCUS);
- Optimization of concrete blends and construction methodologies leveraging concrete's potential to capture carbon and reduce production emissions by up to 23%.

Highlighting the potential to decrease energy demand through mechanical engineering solutions and adopting alternative energy sources, coupled with the considerable capacity of concrete surfaces for CO₂ absorption, it is worthwhile to concentrate on optimizing the clinker-cement ratio for road concretes.

In Europe, 44% of cement production comprises Portland cement composite, with blast furnace and pozzolanic cement contributing 12%. The estimated thermal energy savings and emission reductions achieved through blended cement range from 0.009 to 1.4 GJ per ton and 0.3 to 213.54 kg CO₂ per ton, respectively [6].

In the publication [12], a study was carried out on the lifecycle greenhouse gas emissions associated with different cement mixes, considering factors such as carbonation and durability. Their analysis involved the addition of blast furnace slag and fly ash to clinker, revealing that more substantial reductions in emissions were attainable with blast furnace slag. This is primarily because the proportion of Portland cement replaceable by fly ash is lower than that of blast furnace slag replaceable by fly ash. The most significant impact was observed with an 80% substitution of blast furnace slag, resulting in a remarkable 70% reduction in production stage emissions. Meanwhile, fly ash mixtures achieved a 36% reduction compared to Portland cement when replacing 35% of the clinker. Comparing cement with equal substitution amounts for both blast furnace slag and fly ash indicated that fly ash usage is more environmentally favourable. Fly ash involves fewer downstream processes (e.g., grinding) compared to blast furnace slag, resulting in lower emissions. However, it is essential to note that the article calculated considerably longer transport distances for blast furnace slag (1640 km) in contrast to fly ash (180 km).

Karadumpa and Pancharathi [13] present the energy consumption of different types of cement in five different manufacturing plants in India. It is shown that the 15% fly ash (FA) content in the Portland cement leads to an average 14,69% lower energy consumption than the reference Portland cement (OPC). In the case of the highest examined granulated blast furnace slag (GBFS) content studied (45%), the average energy reduction was 35,29%. The study also examines the composite cements' energy reduction, combining 20% or 25% FA with 20%, 30%, or 35% GBFS content. The highest energy reduction was obtained with 45% OPC+20%FA+35%GBFS with an average of 47%.

Anastasiou et al. [14] investigated the environmental impact of concrete pavements in Greece, incorporating fly ash and slag across six variants. The energy input per kg to produce the clinker, cement, limestone, fly ash, steel slag, and concrete was presented in the paper, where the data was collected from the relevant industries in the region of Northern Greece. Results show significant CO₂ emission reduction compared to standard concrete pavements, with fly ash substitution remaining beneficial even over long distances.

The study by [15] analyses 20 papers (2017-2022) on blast furnace slag as cement replacement in pavements. The article provides a useful overview of the values of the physical properties of OPC, GBFS, and BFS, such as specific gravity, surface area and loss on ignition, and the chemical composition of the materials. It gives a summary of the results of the different replacement methods based on the papers analysed. They found that 50-70% substitution was satisfactory, with 60% being the most common. Only 7 papers addressed cost and eco-efficiency, suggesting that 60% GGBFS replacement could

reduce embodied energy by 37% and CO_2 emissions by 48% compared to control measures.

In Germany, the average clinker-cement ratio was approximately 71% in 2017, indicating that, on average, cement production comprised 71% clinker. Substituting clinker with alternative primary components like granulated blast furnace slag (from flv the steel industry) or ash energy/conversion sources) within the clinker rotary kiln process leads to fuel conservation required for clinker production [16]. This results in an environmentally and energy resource-conscious solution, aiding the concrete industry in striving toward its objectives of achieving carbon neutrality, energy efficiency, and cost-effectiveness. (Kurhan [17] demonstrated that entropy-based simulation techniques could effectively model the stability of railway ballast, and similar methodologies could be explored to assess the energy dynamics within concrete pavement layers.)

German Cement Works Association demonstrates in its publication [18] the impact of increasing blast furnace slag content on CO2 emissions in cement production. Fig. 1. illustrates this impact, indicating that while emissions for CEM I (Portland cement) are estimated to be around 0.9 CO₂/t of cement, emissions for CEMIII/B (blast furnace slag cement), the emissions of CEMIII/B (blast furnace slag cement), which contains 80% blast furnace slag and is the maximum permissible level according to the Hungarian standard e-UT 06.03.37 [19], are below 0.3 CO₂/t of cement. The figure also depicts that the electrical energy demand remains relatively constant with increased blast furnace slag content, attributed to the 'savings' from reducing clinker burning and substituting primary raw materials.

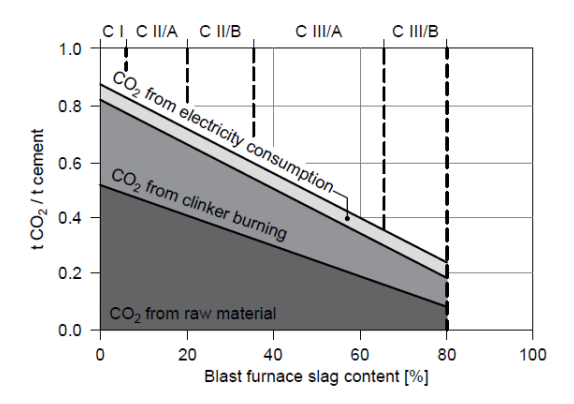


Figure 1. Comparison of CO₂ emissions from the production of blast furnace slag cement and Portland cement, VDZ [17]

Both fly ash and blast furnace slag additive cements are accessible in Hungary, and their impact on concrete is widely recognized. The types of cement admixtures utilized in Hungarian cement production include:

- fly ash Nyitranovák (SK), Visonta, Oroszlány;
- blast furnace slag Kassa (SK), Dunaújváros.

The upcoming paragraph III.1 outlines the alternative cement variations approved by the Hungarian Standards for constructing concrete road structures.

III. VARIETIES OF CEMENT FOR CONCRETE PAVEMENTS IN HUNGARY

Clause 8.2.1 of the relevant Hungarian specification 'Design and Construction of Concrete and Composite Pavements' (e-UT 06.03.37:2021, [19]), stipulates the selection of cement type aligned with Hungarian Standard MSZ 4798 [20] and corresponding to the specified concrete types. According to the specification and MSZ EN 197-1 [21], the permitted cements applicable for concrete pavements include:

- portland cement: CEM I 42.5; CEM I 32.5 and CEM I 32.5N LH;
- blast furnace slag Portland cement: CEM II/A-S 42.5; CEM II/A-S 32.5; CEM II/B-S 42.5 and CEM/II B-S;
- fly ash Portland cement: CEM II/A-V 42.5 and CEM II/A-V 32.5;
- blast furnace slag cement: CEM III/A 32.5 N-M-SR, CEM III/A 32.5 R-M-SR and CEM III/B 32.5 N-SR.

The third element within these symbols (A, B) denotes the proportions of the mixture's components, which include:

- CEM II "A" 6-20%;
- CEM II "B" 21-35%;
- CEM III "A" 36-65%;
- CEM III "B" 66-80%.

Nevertheless, the regulation also specifies that the blending material content in fly ash Portland cement (CEM II/A-V) should not surpass 10 percent of the cement mass. While there are no further specifications in the standard, blast furnace slag Portland cement (composite Portland cement) permits up to a 35% replacement. In the case of blast furnace slag cement (CEM III/B), this replacement rate can reach up to 80%. Typically, manufacturers anticipate a blast furnace slag content of around 75% for CEM III/B, utilizing the standard's allowance of 5%t for other materials in the mixture.

However, it is essential to note that within exposure class XF4 (characterized by high water saturation and the requirement for ice melting agents or seawater), only blast furnace slag cement of type CEM III/A 42.5 N or CEM III/A 32.5 R, containing a blast furnace slag major constituent of less than 50% by weight, is permissible for use [22].

According to the German General Circular for Road Construction (Allgemeine Rundschreiben Strassenbau Deutschland, ARS 04 2022), the following cement types can be utilized, from those available as per DIN EN 197-1, for road paving, with the contractor's consent: CEM II/B-S, CEM II/A-T, CEM II/B-T, CEM II/A-LL, CEM III/A (with a maximum blast furnace slag content of 50% and a minimum strength class of 42.5 N) [3,23]. Considering the more advantageous availability of limestone in Hungary, it would be advisable to explore its potential use (CEM II/A-LL) in cement mixtures for concrete road pavement structures in Hungary.

IV. ENERGY DEMAND OF CONCRETE PAVEMENTS FOR COMPLEX PORTLAND CEMENT AND BLAST FURNACE SLAG CEMENT

Concrete production is a complex, energy-intensive process. **Fig. 2**. illustrates key aspects of the concrete life cycle. A comprehensive understanding of these processes can be found in the article titled 'Energy demand assessment of domestic pavement structures' [4]. The article gathered pertinent energy data from literature sources, such as [24-32], concerning raw material extraction, cement production, concrete mixing, and various raw material production. The average energy values derived from this data collection include:

- production of Portland cement: 6.04×10⁹ [J/t];
- mining of additives: 41.67×10^6 [J/t];
- concrete plant and the mixing: 7.67×10⁶ [J/t].

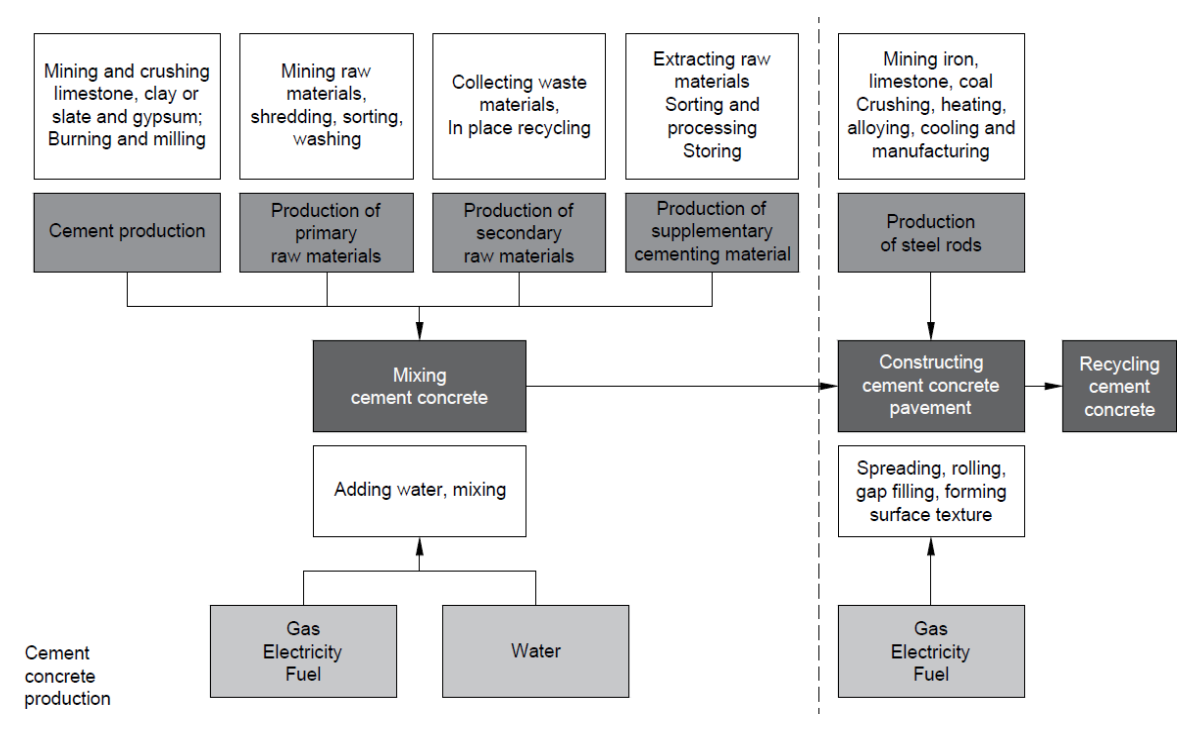


Figure 2. Production of Concrete Mix and Life Cycle Components

On the basis of the values provided, it is clear that the production of Portland cement requires the highest energy input $(6.04\times10^9 \text{ [J/t]})$, which is significantly higher than the energy required for the production, i.e., the mixing of the concrete mixture $(7.67\times10^6 \text{ [J/t]})$.

Furthermore, the paper [4] compared the energy requirements between concrete pavements and asphalt pavements designed for the same traffic category. The findings reveal that, on average, concrete pavements exhibit a 60% higher energy demand, primarily attributed to cement production. However, it is essential to note that these results represent the specific energy demands observed in

the case study, and variations in pavement structure combinations might yield slightly different outcomes.

The aim of the present paper is to recompute the calculations for fly ash Portland cement and blast furnace slag cement. The model assumes the maximum permissible content of blended material outlined in the standard [19]. The calculation does not account for the potential addition by the manufacturer of other materials up to 5% in addition to clinker, gypsum, and the specific additive being studied (blast furnace slag or fly ash). **Fig. 3**. illustrates a simplified depiction of the production process chain.

To ensure comparability of the obtained results, this article also adopts the energy demand of 6.04×10^9 [J/t] for Portland cement production. Based on the article by Huntzinger and Eatmon [33], the estimated energy demand for Portland cement production can be broken down as follows:

- raw material extraction: 5%;
- thermal energy demand: 70%;
- electric power: 25%.

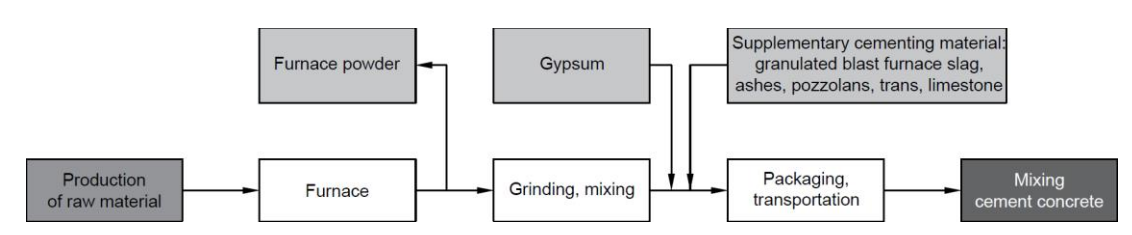


Figure 3. Illustration of Cement Production Processes with blending material

As the preceding literature cited in this article – i.e. [6,10,12,18] – has presented a range of electricity demand from 12% to 38% and thermal energy demand from 62% to 88%, this study adopts averages that align with the findings of Huntzinger and Eatmon [31]. Consequently, the estimated energy demand for cement production is applied as follows:

Raw material extraction: 0.302×10⁹ [J/t]
 Thermal energy demand: 4.228×10⁹ [J/t]
 Electric power: 1.510×10⁹ [J/t]

The incorporation of additives, such as fly ash and granulated blast furnace slag into clinker is evaluated based on these energy distributions.

1. Procedure for calculation and model's dimensions

The modelled 1 km hypothetical road segment near Budapest in this study adheres to Hungarian standards. It was specifically designed for the "extremely heavy" traffic load class, where the design traffic (TF) F100 surpasses 30,000,000 axle

units. Considering the road class and environmental conditions, the designated speed was set at 110 km/h. The analysed cross-section involved a single traffic lane. As the primary focus of this article is to compare the energy demand of various concrete pavement structures, aspects unrelated to the different pavement designs, such as earthworks or road components like signs, pavement markings, safety elements, and barriers, were excluded from the calculations.

Dimension of the calculated section:

- traffic lane width: 3,75 m;
- number of traffic lanes: 1;
- section length: 1000 m.

The pavement structures have been designed in accordance with the Hungarian regulations of the Technical Specification for Hungarian Roads listed in this Section.

Based on the specified traffic category (extremely heavy), five distinct design alternatives for concrete pavement were examined. This is visually represented in **Fig.4**.

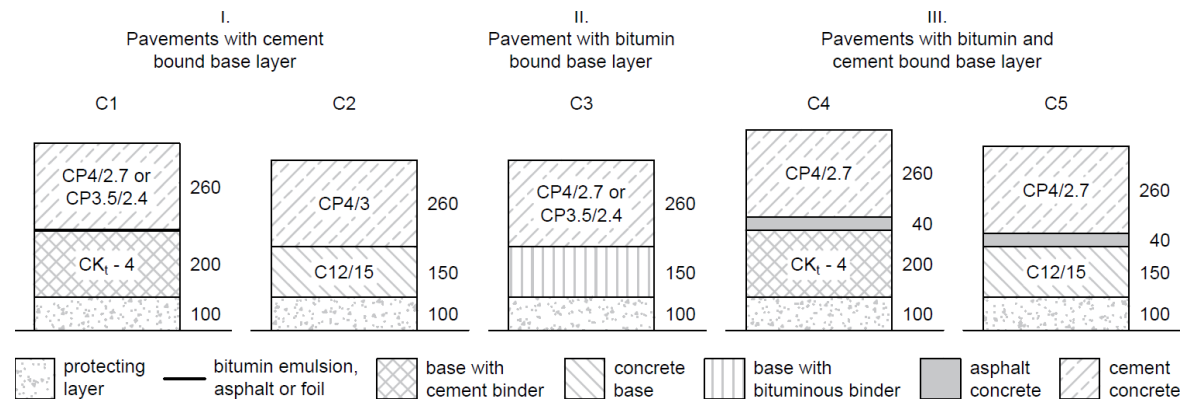


Figure 4. Analysed variations of concrete pavement structures, where CP stands for pavement concrete, C for normal concrete and CKt-4 represents hydraulically bound concrete base layer in C4 quality class

The transportation distance from the mixing plant to the construction site has been established at 50 km, employing heavy goods vehicles with a 32-

tonne capacity. These vehicles will traverse the distance twice, once when fully loaded and once while empty.

According to Stripple's study [28], the diesel consumption of these vehicles is recorded at 0.47 l/km (full) and 0.29 l/km (empty), resulting in energy consumption under these conditions (full and empty) equating to 13.3 MJ/km.

The quantity of load-bearing reinforcement for the concrete pavement remains consistent with the previous article [4], determined in accordance with the applied Hungarian standard specification [19]. Considering the surface area of the section, which measures 3750 m², the calculation indicates that this section necessitates 29,250 kg of reinforcing steel.

Based on the cross-sectional and thickness data, it can also be determined that the section under investigation contains 154 transverse joints. To fill these voids, the article considers employing bitumen-based filling material complying with relevant Hungarian specification e-UT 05.02.42 for Joint Filling Materials of Road Pavements [34].

The mixture design employed for the computation aligns with e-UT 06.03.37:2021 Construction of Concrete Pavements: Specifications, Requirements [19]. Furthermore, the design of the base course aligns with specifications outlined in e-UT 06.03.32 "Concrete Subbases for Road Building: Requirements" [35], e-UT 06.03.33 "Concrete Base Course of Pavement Design Requirements" [36], and e-UT 06.03.53:2018 "Requirements of non-bonded and hydraulic bonded concrete base layers" [37].

2. Energy demand of concrete pavement structures utilizing 10% fly ash-Portland cement

According to Clause 8.2.1 Cement of the specification [19], the article calculates with a maximum permissible fly ash content of 10% of CEM II/A-V fly ash Portland cement. This implies that 10% of the Portland cement clinker is substituted with fly ash. The benefit lies in regarding the production of fly ash as a secondary by-product, which is considered CO₂ emission neutral. Its utilization not only diminishes waste production but also conserves 10% of the substantial thermal energy demand incurred during clinker production. Nevertheless, it is vital to consider the energy

demand associated with transporting the fly ash additive.

In the model, the estimated energy demand for cement production was calculated as follows:

- raw material extraction: $0.302 \times 10^9 \text{ [J/t] (PC)} \rightarrow 0.355 \times 10^9 \text{ [J/t] (VPC)};$
- thermal energy demand: $4.228 \times 10^9 \text{ [J/t] (PC)} \rightarrow 3.805 \times 10^9 \text{ [J/t] (VPC)};$
- electric power: $1.510 \times 10^9 \text{ [J/t] (PC)} \rightarrow 1.359 \times 10^9 \text{ [J/t] (VPC)}.$

Since the Hungarian fly ash sites (Oroszlány, Visonta, Nyitranovák) are situated at varying distances from Budapest (approximately 75 km, 90 km, 215 km), the article approximates an average distance of 100 km. The energy required for transportation is calculated at 13.3 MJ/km for 32-ton trucks, considering one full and one empty run, as per Stripple's research. Consequently, it results in an energy requirement of 2660 MJ for 32 tonnes, roughly equating to 0.083 [J/t]. It has been considered in the energy demand for raw material extraction. The quantity required for producing Portland cement has been adjusted by a 10% reduction to determine thermal and electrical energy demands. Optimization of logistics, such as early garbage collection schedules in urban environments, as studied by Saukenova et al. [38], could similarly be applied to transporting raw materials in road construction, reducing overall energy consumption. The multi-body simulation approach used by Benmeddah et al. [39] for modeling vehicle dynamics could also be adapted to simulate the energy demands of different pavement types, offering more precise predictions and optimizations. As comprehensive data regarding the distribution of grinding and mixing energies in the literature is scarce, further refinement of the model in this aspect may be beneficial.

The calculated energy demand for 10% fly ash Portland cement is roughly equal to 5.519×10^9 [J/t], reflecting an energy saving of 8.63% in comparison to Portland cement $(6.04 \times 10^9 \text{ [J/t]})$.

When transitioning from Portland cement to fly ash Portland cement for C1-C5 pavement types, the energy demands presented in **Table 1.** can be attained.

Table 1. Energy savings in cement production for C1-C5 pavement types using 10% fly asphalt-Portland cement (PC: Portland cement, VPC: fly ash Portland cement)

Pavement structure	Cement quantity [kg]	Energy PC [MJ]	Energy VPC [MJ]	Energy savings [MJ]
C1	675 000.00	4 077 000.00	3 725 325.00	351 675.00
C2	615 937.50	3 720 262.50	3 399 359.06	320 903.44
C3	438 750.00	2 650 050.00	2 421 681.25	228 588.75
C4	675 000.00	4 077 000.00	3 725 325.00	351 675.00
C5	639 562.50	3 862 957.50	3 529 745.44	333 212.06

The values in **Table 1.** represent the life cycle stage of the investigated pavement types until cement production, where Portland cement was substituted by 10% fly ash in the model under investigation. The most substantial savings are notably observed in the C1 and C4 pavement types, which contain the highest cement content. In these

cases, energy savings of up to 3.51×10^4 MJ can be attained.

Table 2 shows the change in energy demand for the entire model, from extraction of raw materials to construction of the road section, for a 10% fly ash substitution.

Table 2. Total energy.	savings l	[%]	for	C1-C5	track	structure	types
-------------------------------	-----------	-----	-----	-------	-------	-----------	-------

Pavement structure	Energy PC [MJ]	Energy VPC [MJ]	%
C1	4 915 169.99	4 563 494.99	7.15
C2	4 428 883.27	4 107 979.83	7.25
C3	3 802 448.60	3 573 858.85	6.01
C4	5 064 576.62	4 712 901.62	6.94
C5	4 741 580.90	4 408 363.83	7.03

The most significant energy savings are observed for the C2 pavement types $(32.09\times10^4[\text{MJ}]; 7.25\%$, followed by C1 and C5. This outcome aligns with expectations, as the C2 pavement types do not contain an asphalt layer. Thus, substituting cement clinker with fly ash can have a greater impact on the total energy demand than the other solutions.

3. Energy demand of concrete track structure with 80% granulated blast furnace slag cement

The literature indicates that while fly ash is considered more environmentally friendly than blast furnace slag due to requiring less additional processing (like grinding), resulting in lower emissions, granulated blast furnace slag can replace a higher percentage of clinker, as per regulations. This is attributed to its latent hydraulic properties, which enhance concrete's resistance to sulphate groundwater.

The paper employs the maximum permissible ratio of 80% slag to clinker for calculation purposes, which determines the estimated energy demand for cement production as follows:

- raw material extraction: 0.302×10⁹ [J/t] (PC) → 1.351×10⁹ [J/t] (SC);
- thermal energy demand: $4.228 \times 10^9 \text{ [J/t] (PC)} \rightarrow 0.846 \times 10^9 \text{ [J/t] (SC)};$
- electric power: $1.510 \times 10^9 \text{ [J/t] (PC)} \rightarrow 0.302 \times 10^9 \text{ [J/t] (SC)}.$

The article also assumes 100 km for transportation distance, accounting for the varying locations of

Hungarian and nearby sites (Kassa, Dunaújváros) from Budapest (approximately 80 km, 265 km). Consequently, an energy value of 0.083×10⁹ [J/t] has been considered in the model's energy demand calculation for raw material extraction.

Little information about the energy requirements for grinding granulated blast furnace slag is available. The distribution of energy requirements has been approximated based on the VDI publication (see Fig. 1). In the model, it is assumed that the grinding energy of blast furnace slag is equal to the grinding energy of clinker. Accordingly, the estimated value for blast furnace slag's energy demand during raw material extraction is 1.291 J/t. Adding this to the energy requirement for clinker raw material extraction results in a total of 1.351×10^9 J/t. To determine the thermal and electricity energy demand, the quantity required for the production of Portland cement has been considered and reduced by 80%. Given the scarcity of precise data on grinding and mixing energy distributions in the available literature, further refinement of the model regarding this aspect might also be beneficial.

The resulting energy demand for the 80% granulated blast furnace cement is 2.499×10^9 [J/t], which resulted in an energy saving of 58.63% compared to Portland cement $(6.04 \times 10^9 \text{ [J/t]})$.

By shifting from Portland cement to blast furnace cement for C1-C5 pavement types, the resulting energy savings are shown in **Table 3**.

Table 3. Energy savings in cement production for C1-C5 pavement types by replacing 80% of Portland cement
with granulated blast furnace slag (PC: Portland cement, SC: Blast furnace slag cement))

Pavement structure	Cement quantity [kg]	Energy PC [MJ]	Energy SC [MJ]	Energy savings [MJ]
C1	675 000.00	4 077 000.00	3 725 325.00	351 675.00
C2	615 937.50	3 720 262.50	3 399 359.06	320 903.44
C3	438 750.00	2 650 050.00	2 421 681.25	228 588.75
C4	675 000.00	4 077 000.00	3 725 325.00	351 675.00
C5	639 562.50	3 862 957.50	3 529 745.44	333 212.06

The values in **Table 3** represent the life cycle stage of the studied road structure types up to cement production. Substituting Portland cement with 80% blast furnace slag, the most significant savings are noted in C1 and C4 pavement types, with higher cement content, yielding up to 23.90×10⁴ MJ. Meanwhile, the highest energy requirement persists in the C4 pavement structure type.

Table 4 shows the change in energy demand for the whole model, from extracting raw materials to constructing the road section. The most significant energy savings are observed for the C2 pavement types ($218.10 \times 10^4 [MJ]$; 49.25%), followed by C1 and C5. This outcome aligns with expectations again since the C2 pavement structure type does not contain an asphalt layer. Therefore, substituting cement clinker with fly ash can have a greater impact on the total energy demand than the other solutions. Meanwhile, the highest energy requirement persists in the C4 pavement structure type.

Table 4. Total energy savings [%] for C1-C5 track structure types

Pavement structure			%
	[MJ]	[MJ]	
C1	4 915 169.99	2 524 994.99	48.63
C2	4 428 883.27	2 247 848.58	49.25
C3	3 802 448.60	2 248 833.85	40.86
C4	5 064 576.62	2 674 401.62	47.19
C5	4 741 580.90	2 476 890.08	47.76

V. COMPARISON OF ENERGY REQUIREMENTS OF ASPHALT AND CONCRETE PAVEMENTS AND POSSIBILITIES FOR FURTHER DEVELOPMENT OF THE MODEL

The comparison between concrete and asphalt pavements in terms of energy requirements is crucial

for evaluating their sustainability and environmental impact. The paper aims to reassess the energy demand of concrete pavement structures on road section R classified under the "extremely heavy" traffic category, using CEM II/A-V and CEM III/B type cement [4]. Asphalt pavement structures used for comparison are shown in **Fig. 5**.

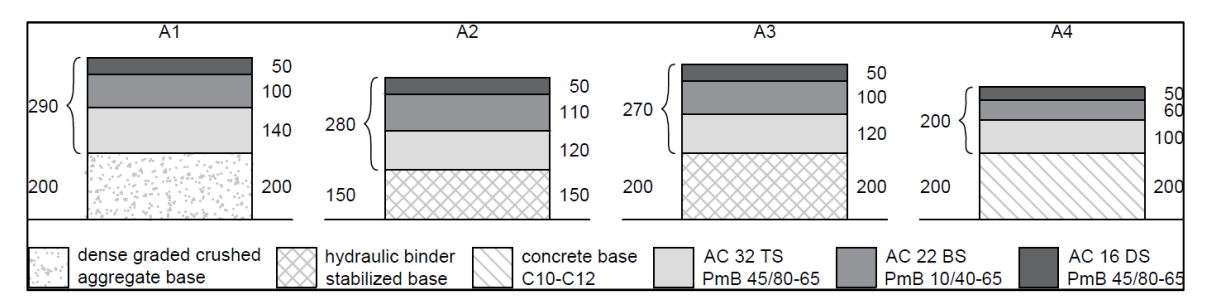


Figure 5. Analysed variations of concrete pavement structures, where PmB means polymer-modified bitumen

While the previous findings [4] suggest that concrete pavements using Portland cement (OPC) require approximately 60% more energy than asphalt

pavements, the results presented in this article for concrete pavement structures are comparable to the energy requirements of asphalt pavements, as demonstrated in **Table 5.**

Pavement structure	Energy-need SC Concrete [MJ]	Pavement structure	Energy-need HMA Asphalt [MJ]
C1	2 524 995	A1	1 430 375
C2	2 247 849	A2	2 335 698

A3

A4

2 248 834

2 674 402

2 476 890

Table 5. Load class R comparison of concrete and asphalt pavement structures applying blast furnace slag cement (SC, 80%)

Looking at **Table 5**, several observations can be made. If we compare these values, we can see that the energy values of the concrete pavements (C1-C5) are similar to those of the asphalt pavements A2-A4, so the concrete pavements with 80% blast furnace slag cement are real competitors of the asphalt pavements in terms of lower energy consumption. Moreover, the results for concrete pavement types C2 and C3 are notably lower than asphalt pavement types A3 and A4. Despite this, it is crucial to note that asphalt pavement type A1 demands significantly (about 63%) less energy.

C3

C4

C5

This finding underlines the importance of pavement design and the potential for optimising energy consumption in the construction of both concrete and asphalt pavements, as well as demonstrates that the negative climate impact of concrete pavements can be reduced using alternative cementitious by-product materials such as fly ash or slag. (As explored by Barać et al. [40], innovative educational platforms for clean production emphasize the importance of incorporating sustainability into engineering curricula, which could lead to more energy-efficient practices in concrete pavement construction.)

The differences presented in **Table 5** can be further nuanced by considering the whole life cycle, where the energy requirements for maintenance and renovation works are included in the model. Furthermore, expanding the model by introducing a cement variation that aligns with environmental class XF4 could be valuable. Additionally, considering the favourable availability of limestone in Hungary, exploring the domestic use of CEM II/A-LL in concrete pavement structures might prove worthwhile. The performance and mechanical properties of concrete pavements with such high levels of blended cements also will require investigation for long-term life cycle objectives.

To compare asphalt and concrete structures, it is also advised to extend the research to the whole life cycle, including the use phase and the end-of-life processes.

VI. CONCLUSIONS

2 766 590

2 465 943

The construction sector, known for its high energy demands and significant CO_2 emissions, notably contributes through cement production [41]. The Paris Agreement aims to limit global warming to 1.5-2.0 °C and achieve carbon neutrality by 2050. In order to achieve this, it is essential to reduce emissions and modernise industries such as construction. Blended cements such as fly ash and blast-furnace slag are used worldwide to replace cement in concrete mixes partially.

In Hungary, fly ash in Portland cement is limited to 10%, while blast-furnace slag cement allows up to 80% replacement of clinker. Calculated with these values, replacing 10% of Portland cement with fly ash in the model shows an energy saving of 8.63% in cement production. This substitution could potentially result in energy savings of up to 7.25% for the pavement structures studied from material extraction to the end of construction. Replacing Portland cement with 80% blast-furnace slag can reduce the energy required for cement production by 58.63%. This change could result in up to 49.25% energy savings for the road structures studied. The result is consistent with the existing literature presented in Section 2. Considering the study examines the highest possible fly ash and blast furnace content, a lower Portland cement replacement to maintain concrete performance in the design situation could still result in relevant costs, waste, natural resources, CO2 emissions, and energy savings.

Both fly ash and granulated blast furnace slag have been widely used in concrete production, but their use in pavements is limited [42,43]. However, even though their mechanical properties and performance have been successfully investigated in numerous publications, such as [44-51], there seems to be some doubt among designers and decision-makers about the use of this technology. After reviewing the literature, it also became clear that relatively few articles investigated the energy saving of blended cement concrete for pavements. One of the aims of this publication is to demonstrate the environmental benefits of using fly ash and blast furnace slag to promote their use in road construction. The results

show that concrete can become an excellent alternative to asphalt pavements in environmental design decisions. As there are environmental, geographical, and regulatory (EU directives and regulations) similarities between Hungary and many European countries (such as Poland, Czech Republic, Slovakia, Germany etc.), the results of this study may be helpful for policymakers in many countries.

AUTHOR CONTRIBUTION

R. Szpotowicz: Conceptualization, Modelling, Calculation, Writing and editing.

REFERENCES

- [1] H. AzariJafari, F. Guo, J. Gregory and R. Kirchain, "Solutions to achieve carbon-neutral mixtures for the U.S. pavement network," The International Journal of Life Cycle Assessment, no. 28(4) (2021). https://doi.org/10.1007/s11367-022-02121-1
- [2] V. Volkov, I. Taran, T. Volkova, O. Pavlenko, and N. Berezhnaya, "Determining the efficient management system for a specialized transport enterprise," Naukovyi Visnyk Natsionalnoho Hirnychoho Universytetu, no. 4, pp. 185-191, 2020. https://doi.org/10.29202/nvngu/2020-4/8
- [3] Hungarian Cement Concrete and Lime Association, Update 62: Durable and safe. Concrete pavements., CeMBeton (2023), in Hungarian
- [4] R. Szpotowicz, Energy demand assessment of Hungarian road structures, Útügyi Lapok, pp. 30-50, (2020) in Hungarian https://doi.org/10.36246/UL.2020.2.03
- [5] CEMBUREAU The European Cement Association, Activity Report, 2021 CEMBUREAU, Brussels (2022). https://cembureau.eu/library/reports/
- [6] N. Madlool, R. Saidur, N. Rahim and M. Kamalisarvestani, An overview of energy savings measures for cement industries, Renewable and Sustainable Energy Reviews, vol. 19, pp. 18-29 (2012). https://doi.org/10.1016/j.rser.2012.10.046
- [7] N. Madlool, R. Saidur, M. Hossain and N. Rahim, A critical review on energy use and savings in the cement industries, Renewable and Sustainable Energy Reviews, vol. 15, pp. 2042-2060 (2011). https://doi.org/10.1016/j.rser.2011.01.005
- [8] J. B. Soares and M. T. Tolmasquim, Energy efficiency and reduction of CO2 Emissions through 2015: The Brasilian cement industry, Mitigation and Adaptation Strategies for Global Change, vol. 5, pp. 297-318 (2000). https://doi.org/10.1023/A:1009621514625

C. Tóth: Conceptualization, Supervision, Review.

DISCLOSURE STATEMENT

The authors declare that they have no known competing financial interests or personal relationships that could have appeared to influence the work reported in this paper.

ORCID

Réka Szpotowicz: http://orcid.org/0000-0003-1507-6174

Csaba Tóth: http://orcid.org/0000-0001-5065-5177

- [9] A. Dodoo, L. Gustavsson and R. Sathre, Carbon implications of end-of-life management of building materials, Resources, Conservation and Recycling, p. 276–286 (2009). https://doi.org/10.1016/j.resconrec.2008.12.00
- [10] N. Pardo, J. A. Moya and A. Mercier, Prospective on the energy efficiency and CO2 emissions in the EU cement industry, Energy, vol. 36, pp. 3244-3254 (2011). https://doi.org/10.1016/j.energy.2011.03.016
- [11] R. Kumar, E. Althaqafi, S. G. K. Patro, V. Simic, A. Babbar, D. Pamucar, S. K. Singh, and A. Verma, "Machine and deep learning methods for concrete strength prediction: A bibliometric and content analysis review of research trends and future directions," Applied Soft Computing, vol. 164, 111956, 2024. https://doi.org/10.1016/j.asoc.2024.111956
- [12] T. García-Segura, V. Yepes and J. Alcalá, Life cycle greenhouse gas emission of blended cement concrete including carbonation and durability, The International Journal of Life Cycle Assessment, vol. 19, pp. 3-12 (2014). https://doi.org/10.1007/s11367-013-0614-0
- [13] C. S. Karadumpa and R. K. Pancharathi, Study on energy use and carbon emission from manufacturing of OPC and blended cements in India, Environmental Science and Pollution Research, p. 5364–5383 (2024). https://doi.org/10.1007/s11356-023-31593-3
- [14] E.K. Anastasiou, A. Liapis and I. Papayianni, Comparative life cycle assessment of concrete road pavements using industrial by-products as alternative materials, Resources, Conservation and Recycling 101, pp. 1-8, (2015). https://doi.org/10.1016/j.resconrec.2015.05.00
- [15] L. H. Pereira Silva, V. Nehring, F. F. Guedes de Paivaa, J. R. Tamashiro, A. P. Galvín and A. López-Uceda, Use of blast furnace slag in cementitious materials for pavements -

- Systematic literature review and ecoefficiency, Sustainable Chemistry and Pharmacy, pp. 1-9 (2023).
- https://doi.org/10.1016/j.scp.2023.101030
- [16] D. M. Kurhan, "Entropy Application for Simulation the Ballast State as a Railway Element," Acta Polytechnica Hungarica, vol. 20, no. 1, pp. 63-77, 2023. https://doi.org/10.12700/APH.20.1.2023.20.5
- [17] Bundesministerium für Wirtschaft und Energie, Energiewende in der Industrie: Potenziale und Wechselwirkungen mit dem Energiesektor, Branchensteckbrief der Zement- und Kalkindustrie, Navigant Energy Germany GmbH (2020), in German
- [18] Verein Deutsche Zementwerke, CEM II- und CEMIII/A- Zemente im Betonbau, Nachhaltige Lösunden für das Bauen mit Beton, Düsseldorf (2008), in German
- [19] Útügyi Műszaki Előírás/Hungarian Technical Specifications for Roads, Design and Construction of Concrete and Composite Pavements / Beton- és kompozitburkolatok tervezése és építése, e-UT 06.03.37:2021 (2021) in Hungarian
- [20] Hungarian Standards Institution, Concrete. Specification, performance, production and conformity and conditions of application of EN 206 in Hungary (2021).
- [21] Hungarian Standards Institution, MSZ EN 197-1:2011, Cement Composition, specifications and conformity criteria for common cements (2011), in Hungarian
- [22] Hungarian Cement Concrete and Lime Association, CEMBETON Guidance 2017, Budapest: Magyar Cement-, Beton- és Mészipari Szövetség (2017), in Hungarian
- [23] Bundesministerium für Digitales und Verkehr, General Circular for Road Construction / Allgemeines Rundschreiben Straßenbau Nr. 04/2022 (StB 25/7182.8/3-ARS-22/3644896), Bonn (2022), in German
- [24] E. Anastasiou, A. Liapis and I. Papayianni, Comparative life cycle assessment of concrete road pavements using industrial by-products as alternative materials, Resources, Conservation and Recycle, pp. 1-8 (2015). https://doi.org/10.1016/j.resconrec.2015.05.00
- [25] R. J. Stammer and F. Stodolsky, Assessment of the Energy Impacts of Improving Highway-Infrastructure Materials, Center for Transportation Research, Argone National Laboratory, Illinois (1995). https://doi.org/10.2172/177967
- [26] J. Chehovits and L. Galehouse, Energy Usage and Green House Gas Emission of Pavement Preservation Processes for Asphalt Concrete Pavements, Compendium of Papers from the

- First International Conference on Pavement Preservation, pp. 27-42, 15 4 (2010) Corpus ID: 106462011.
- [27] T. Häkkinen and K. Mäkelä, Environmental adaptation of concrete: Environmental impact of concrete and asphalt pavements, VTT, Technical research centre of Finland (1996). https://publications.vtt.fi/pdf/tiedotteet/1996/T 1752.pdf
- [28] H. Stripple, Life Cycle Assessment of Road; A Pilot Study for Inventory Analysis, Swedish National Road Administration, Gothenburg, Sweden (2001). https://www.diva-portal.org/smash/record.jsf?pid=diva2%3A15 50976&dswid=-3669
- [29] Athena Institute, A life cycle perspective on concrete and asphalt roadways: Embodied primary energy and global warming potential, Cement Association of Canada, 2006.
- [30] F. Gschösser, H. Wallbaum and M. E. Boesch, Life-cycle assessment of the production of Swiss road materials, Journal of materials in civil engineering vol. 24 (2), pp. 168-176 (2012). https://doi.org/10.1061/(ASCE)MT.1943-5533.0000375
- [31] M. Chappat and J. Bilal, Environmental Road of the Future: Life cycle Analysis, Energy Consumption and Greenhouse Gas Emissions, Proceedings of the Fiftieth Annual Conference of the Canadian Technical Asphalt Association (CTAA) in Victoria, British Columbia, pp 1-26 (2005). https://trid.trb.org/View/849158
- [32] P. Zapata and J. A. Gambatese, Energy consumption of asphalt and reinforced concrete pavement materials and construction, Journal of Infrastructure Systems, vol. 11, pp. 9-20 (2005). https://doi.org/10.1061/(ASCE)1076-0342(2005)11:1
- [33] T. D. E. Deborah N. Huntzinger, A life-cycle assessment of Portland cement manufacturing: comparing the traditional process with alternative technologies, Journal of Cleaner Production, pp. 668–675 (2008). https://doi.org/10.1016/j.jclepro.2008.04.007
- [34] Útügyi Műszaki Előírás/Hungarian Technical Specifications for Roads, e-UT 05.02.42 Joint Filling Materials of Road Pavements (2008) in Hungarian
- [35] Útügyi Műszaki Előírás/Hungarian Technical Specifications for Roads, e-UT 06.03.32 Concrete Subbases for Road Building Requirements, (1993) in Hungarian
- [36] Útügyi Műszaki Előírás/Hungarian Technical Specifications for Roads, e-UT 06.03.33 Concrete Base Courses of Pavement Design Requirement (2008) in Hungarian

[37] I. Saukenova, M. Oliskevych, I. Taran, A. Toktamyssova, D. Aliakbarkyzy, and R. Pelo, "Optimization of schedules for early garbage collection and disposal in the megapolis," Eastern-European Journal of Enterprise Technologies, vol. 1, no. 3(115), pp. 13-23, 2022.

https://doi.org/10.15587/1729-4061.2022.251082

- [38] A. Benmeddah, V. Jovanović, S. Perić, M. Drakulić, A. Đurić, and D. Marinković, "Modeling and Experimental Validation of an Off-Road Truck's (4 × 4) Lateral Dynamics Using a Multi-Body Simulation," Applied Sciences, vol. 14, p. 6479, 2024. https://doi.org/10.3390/app14156479
- [39] M. Barać, N. Vitković, Z. Stanković, M. Rajić, and R. Turudija, "Description and Utilization of an Educational Platform for Clean Production in Mechanical Engineering," Spectrum of Mechanical Engineering and Operational Research, vol. 1, no. 1, pp. 145-158, 2024. https://doi.org/10.31181/smeor11202413
- [40] Útügyi Műszaki Előírás/Hungarian Technical Specifications for Roads, e-UT 06.03.53:2018 Requirements of non-bonded and hydraulic bonded concrete base (2018) in Hungarian
- [41] Our Word in Data, https://ourworldindata.org, 2019, [cited 2023-07-30].
- [42] Our Word in Data, https://ourworldindata.org, 2021, [cited 2023-07-30]. https://ourworldindata.org/grapher/annual-co2
 - cement?time=earliest..latest&country=~HUN
- [43] S. Pranav, S. Aggarwal, E.-H. Yang, A. K. Sarkar, A. P. Singh and M. Lahoti, Alternative materials for wearing course of concrete pavements: A critical review, Construction and Building Materials, vol. 236, (2020). https://doi.org/10.1016/j.conbuildmat.2019.11 7609
- [44] Y. Aoki, R. Sri Ravindrarajah, and H. Khabbaz, Properties of pervious concrete containing fly ash', Road Materials and Pavement Design, vol 13(1), pp. 1–11 (2012)

- https://doi.org/10.1080/14680629.2011.65183
- [45] X. Chen, H. Wang, H. Najm, G. Venkiteela and J. Hencken, Evaluating engineering properties and environmental impact of pervious concrete with fly ash and slag, Journal of Cleaner Production, vol. 237 (2019). https://doi.org/10.1016/j.jclepro.2019.117714
- [46] M. N.-T. Lam, D.-H. Le and S. Jaritngam, Compressive Strength and Durability Properties of Roller-Compacted Concrete Pavement containing Electric Arc Furnace Slag Aggregate and Fly Ash, Construction and Building Materials, pp. 912-922 (2018). https://doi.org/10.1016/j.conbuildmat.2018.10.080
- [47] P. Suraneni, V. J. Azad, O. Isgor and W.J. Weiss, Use of Fly Ash to Minimize Deicing Salt Damage in Concrete Pavements, Transportation Research Record, 2629(1), pp. 24-32 (2017) https://doi.org/10.3141/2629-05
- [48] A. Aghaeipour and M. Madhkhan, Effect of ground granulated blast furnace slag (GGBFS) on RCCP durability, Construction and Building Materials, vol. 141, pp. 533-541 (2017). https://doi.org/10.1016/j.conbuildmat.2017.03.
- [49] L. Nicula, O. C. Corbu and M. Iliescu, Influence of Blast Furnace Slag on the Durability Characteristic of Road Concrete Such as Freeze-Thaw Resistance, Procedia Manufacturing, vol. 46, pp. 194-201 (2020). https://doi.org/10.1016/j.promfg.2020.03.029
- [50] G. L. Golewski, Energy Savings Associated with the Use of Fly Ash and Nanoadditives in the Cement Composition, Energies, vol. 13(9), pp. 1-20 (2020) https://doi.org/10.3390/en13092184
- [51] J. Skarabis and C. Gehlen, "Durability of pavements concrete made with fly ash, 3rd International fib Congress and Exhibition, Incorporating the PCI Annual Convention and Bridge Conference 2010 (2010).



This article is an open access article distributed under the terms and conditions of the Creative Commons Attribution NonCommercial (CC BY-NC 4.0) license.



ACTA TECHNICA JAURINENSIS

Vol. 17, No. 3, pp. 130-142, 2024 10.14513/actatechjaur.00746



Research Article

Processing Spatial Data for Statistical Modelling and Visualization Case study: INLA model for COVID-19 in Alabama, USA

Getachew Dejene^{1,*}, György Terdik²

¹ Doctoral School of Informatics, University of Debrecen, 4028, Debrecen, Hungary ² Department of Information Technology, Faculty of Informatics, University of Debrecen, 4028, Debrecen, Hungary *e-mail: engidaw.getachew@inf.unideb.hu

Abstract: This research emphasizes the visualization of spatial data for statistical modelling and analysis of the relative risk associated with the COVID-19 pandemic in Alabama, USA. We used Bayesian analysis and the Integrated Nested Laplace Approximation (INLA) approach on data ranging from March 11, 2020, to December 31, 2022, which included observed COVID-19 cases, the population for each of the Alabama counties, and a Geographical map of the state. The geographical distribution of COVID-19's relative risk was determined using various spatial statistical techniques, indicating high-risk locations. The study used Besag-York-Mollié (BYM) models to assess the posterior relative risk of

COVID-19, and it found a statistically significant average decrease in COVID-19 case rates across the 67 counties evaluated. These findings have practical implications for evidence-based policymaking in pandemic prevention, mitigation, and preparation.

Keywords: COVID-19; Spatial Data; Disease mapping; Bayesian analysis; hot spot

I. Introduction

Spatial statistics revolves around the fundamental concept of spatial processes, which involves comprehending and modelling the variations of variables or phenomena across different spatial locations [46]. This concept is essential for capturing and analysing spatial dependencies and patterns exhibited by the variable of interest. In the context of the global COVID-19 pandemic, understanding the spread and impact of the virus is crucial for effective decisionmaking, resource allocation, and public health interventions [26]. Spatial data and modelling techniques provide a powerful approach to gaining insights into the dynamic nature of the pan-demic [49]. Spatial data about COVID-19 goes beyond temporal trends by considering the geographic location and spatial relationships of cases, deaths, and other relevant variables [31]. This encompasses data on COVID-19 cases, hospitalizations, deaths, testing rates, and vaccination coverage collected at various geographical resolutions, such as countries, states, counties, or smaller administrative units. By incorporating the spatial dimension, analysts can examine patterns, clusters, and disparities in the spread and impact of the virus across different regions [16]. Spatial modelling techniques enable researchers to explore and analyse spatial data, facilitating the identification of underlying patterns, assessing spatial dependencies, and predicting. These models consider spatial relationships and autocorrelation, recognizing that nearby locations are likely to exhibit similar values due to shared characteristics or proximity [29, 50]. By considering spatial effects such as the spatial spread of infections or the influence of local contextual factors, spatial models improve prediction accuracy and offer valuable insights for policymakers, healthcare professionals, and the general public [23]. COVID-19 spatial modelling encompasses a wide range of approaches [14]. One commonly used technique is spatial clustering analysis, which identifies areas with concentrated high or low COVID-19 incidence, aiding in targeted interventions and resource allocation. Other modelling approaches include graphically Weighted Regression, which accounts for spatial heterogeneity in the relationship between Covid-19 outcomes and potential predictors, and spatial auto-regressive models such as spatial lag or spatial error models, which capture spatial dependencies among neighbouring regions [18, 30, 48]. In addition to analysing the spread of the virus, spatial modelling can also assess the impact of interventions and policies. By integrating spatial data on containment measures, vaccination campaigns, or mobility restrictions, researchers can evaluate their effectiveness and explore spatial variations in out- comes. Spatial statistics, at its essence, entails com-prehending and modelling the variations of variables or phenomena, while also capturing and representing the outcomes or observations linked to spatial locations [28]. The data can be represented as measurements conducted at spatial units within a fixed spatial domain. This domain can be either a continuous surface or a countable collection of spatial units, such as census tracts or ZIP codes [6]. Areal data is generated through the division of a fixed geographic region into smaller sub-regions, which act as units for aggregating diverse outcomesor events [7]. This type of data finds applications across various fields, including the assessment of cancer cases in different counties [32], the docu- mentation of road accidents in various provinces [38], and the measurement of the proportion of individuals living below the poverty line in census tracts [40]. Researchers can analyse and understand patterns and trends within specific sub-regions by utilizing areal data, enabling insights and informed decision-making in these respective domains.

In this study, we focus on examining the spatial pattern of Standardized Incidence Rate of COVID-19 observed across the 67 Alabama Counties rather than individual points. The variable of interest represents a suitable summary, such as the number of case rates within each respective area. **Fig. 1** presents the Population distribution of Alabama in 67 counties in, the USA.

1. Related works

The COVID-19 pandemic demanded the quick development and implementation of new statistical approaches for modelling and predicting viral propagation [1]. Bayesian analysis and the INLA method have emerged as useful techniques for dealing with complicated spatial and spatio-temporal data [36, 44, 52].

Bayesian analysis and the INLA method have proven essential in tackling the complex spatial and spatio-temporal data associated with COVID-19. These techniques enable the incorporation of prior information and hierarchical structures, offering robust frameworks to handle the uncertain- ties and variability in epidemiological data. For instance, hierarchical Bayesian models have been applied to COVID-19 case data in Bangladesh to account for spatial autocorrelation, thus identifying clusters of high prevalence and providing more accurate risk assessments [22].

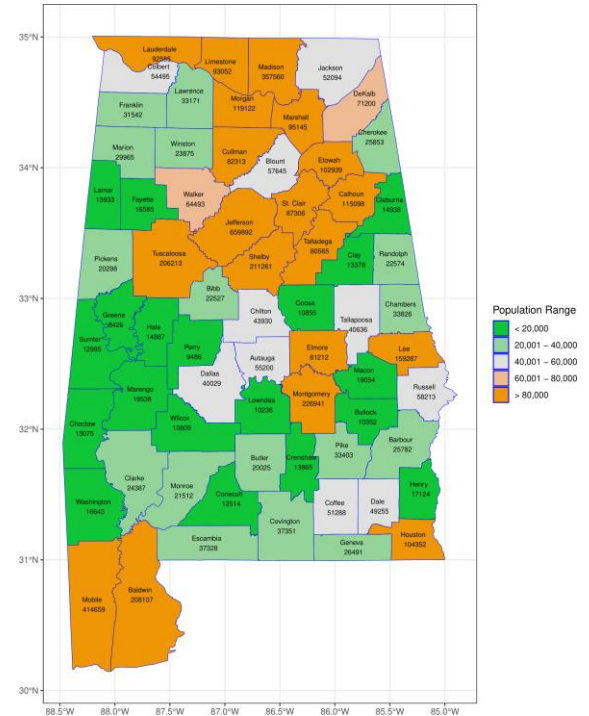


Figure 1. Population distribution of Alabama per county

Similarly, in Europe, spatio-temporal Bayesian models have been utilized to study the spread and control measures' impact across Spain, Italy, and Germany, demonstrating how these models can inform public health decisions by capturing the temporal dynamics and spatial heterogeneity of the pandemic [20]. Furthermore, addressing data reporting issues, hierarchical Bayesian models correct misreporting in the U.S., enhancing the reliability of spatial risk estimates [10]. As far as the authors are aware, this research represents the pioneering effort in utilizing visualization techniques for spatial data in the con-text of statistical modelling and analysis of the relative risk linked to the COVID-19 pandemic specifically in Alabama, USA, using Bayesian analysis coupled with the INLA method.

2. Spatial Data

Spatial data can be described as outcomes or observations of a random process that is associated with specific spatial locations [5, 46]:

$$Y \equiv \{y(s), s \in D\} \tag{1}$$

where Y represents a set of measurements conducted at the spatial units' s D. The subset D in R^d (d=2 in this context) establishes the spatial domain. Using the characteristics of the domain D, spatial data can be categorized as areal (or lattice) data, geo statistical data, or point patterns data.

Areal or lattice data is a type of spatial data that emerges when a specific geographic region, known as a fixed domain, is divided into a finite number of sub-regions [3]. These sub-regions serve as units for aggregating various outcomes or events. Areal data find applications in a range of fields and can be found in diverse contexts. Understanding the data's structure is crucial because specific analytical methods are better suited for certain data types. Being aware of the data's characteristics helps in selecting the most suitable analytical approaches.

In the case of data referring to areas, the location of each object needs to satisfy an agreed convention [19]. If the areas are irregular shapes, then one options is to select a representative point such as the area or population-weighted centroid, and then use the same procedure as for a point object to provide s_i . Alternatively, each area can be labelled, and alookup table can be provided to match rows of the data matrix to the corresponding areas on the map.

In disease mapping, the fundamental situation involves utilizing spatial data specifically related to distinct, non-overlapping *n* sub-regions [12]. A few examples of areal data include the count of cancer cases in different counties, the number of road accident reported in various provinces, and the proportion of people living below the poverty line in census tracts [34], etc. In each case, the fixed domain, such as a county, province, or census tract, is divided into smaller sub-regions, enabling the aggregation of relevant information within those subregions. In general, data related to a specific area are often observed and recorded within spatially aggregated domains, such as administrative geographies like postcodes, counties, or districts.

Rather than focusing on specific locations, Our study encompasses all 67 counties in Alabama, utilizing a dataset obtained from the official Kag- gle repository source. The dataset contains dailyupdated information on reported cases and deaths in the United States, documented at both state and county levels. The dataset consists of two primary CSV files: 'covid us county.csv,' containing columns such as fips, county, state, latitude, long, date. cases. state-code, and deaths: 'us county.csv,' featuring columns like fips, county, state, state-code, male, female, median-age, population, female-percentage, latitude, and long. Addition- ally, the collection includes US county shape files for geospatial plots in formats like 'us county.shp,' 'dbf,' 'prj,' and 'shx'.

However, the earliest reported incidents in the original dataset traced back to January 22, 2020. For the scope of our study, which centred on the state of Alabama, we rigorously filtered the information, yielding a total of 1,024 records. During the preprocessing and cleaning step, certain entries were eliminated, notably those with duplicate geoidentifier fields and unsigned county values. Our investigation is limited to the period between March

11, 2020, and December 31, 2022, encapsulating the period with the first nonzero values. The refined dataset will be employed in our analysis, emphasizing key fields such as county (the English name for the county), longitude, latitude (geographic co- ordinates of the region's centroid), cases (number of confirmed COVID-19 cases), population (population of the county), and geometry (polygon de- scribing the geographical area).

3. Data Processing and plot Generation for COVID-19 Dataset Analysis

In the data processing and categorization phase of our COVID-19 dataset analysis, we utilized the R programming language, leveraging key packages like "Simple Features in R" (sf), more over a set of packages called "tidyverse" that share a high-level design philosophy and low-level grammar and data structures [54]. The "sf" package facilitated spatial data manipulation, notably through the st sf() function, creating spatial data frames with seamless geographic integration. Functions like st read() and st write () ensured efficient reading and writing of spatial data in various formats. Concurrently, the "tidyverse" package, encompassing vitalR packages, streamlined general data manipulation tasks. Functions from "dplyr" within the tidyverse, such as filter (), mutate (), and summarize (), played acrucial role in non-spatial data processing, ensuring a consistent and efficient methodology. The technical integration of "sf" and "tidyverse" contributed to a well-structured approach in handling both spatialand non-spatial aspects of the COVID-19 dataset.

Understanding the organization of COVID-19 data frames is crucial for accurately analysing and interpreting pandemic-related information. **Fig. 2** illustrates the fundamental structure of the COVID-19 data frame and the method for man- aging Alabama county shapefiles.

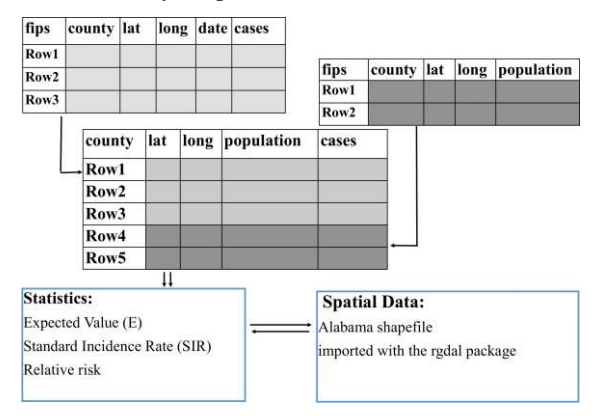


Figure 2. Structure of Covid-19 Data frame and Alabama county shapefile process.

Additionally, it highlights the key statistical functions utilized for data analysis. In this process, we merge these two tables using a shared key aligned with our researchobjectives. This merging approach

pertinent data from both allows us to integrate sources, facilitating a more comprehensive investigation and interpretation of COVID-19 trends at the county level. By amalgamating data from the COVID-19 data frame with Alabama county shapefiles, we are equipped to get insights into the geographical distribution of cases, demographics, and other relevant factors influencing pandemic's trajectory.

To enhance the presentation of selected data such as COVID-19 cases, expected cases, SIR, and relative risk, we apply a statistical technique:

$$gr[1] = min + \frac{median - min}{2.5}$$
 (2)

$$gr[1] = min + \frac{median - min}{2.5}$$

$$gr[2] = min + 2\left(\frac{median - min}{2.5}\right)$$
(3)

$$gr[3] = max - 2\left(\frac{max - median}{2.5}\right)$$
 (4)

$$gr[4] = max - \frac{max - median}{2.5}$$
 (5)

following the consolidation of all data frames. This technique involves defining groups (denoted as gr) using quartile splits, incorporating statistical measures like minimum (min), maximum (max), and median.

The vector "gr" plays a pivotal role in capturing these quartile breakdowns, facilitating more de-tailed data segmentation and analysis. Quartile borders are determined systematically as follows: - The lower boundary of the first quartile, gr[1], is computed by adding a fraction of the range between thelowest and median to the minimum value. The up-per boundary of the first quartile, gr[2], expands proportionally on that range. Similarly, the lower boundary of the third quartile, gr[3], is calculated by subtracting twice the proportion of the range be-tween the maximum and median from the highest value. In contrast, the upper boundary, gr[4], is determined by deducting the fraction of that range. The resulting rounded values of gr (rounded tothree decimal places) lead to the segmentation of the dataset into five distinct groups: "Very Low," "Low," "Medium," "High," and "Very High," basedon the distribution of "confirmed cases" versus "expected cases". This approach ensures a fair and meaningful classification, contributing to a comprehensive understanding of the variables' distribution within the dataset.

II. METHODOLOGY

The dataset, sourced from Kaggle, underwent initial filtration to focus specifically on Alabama counties ties. Subsequently, relevant information about population, COVID-19 cases, and counties was systematically extracted and organized. To enhance data interpretability, temporal considerations were integrated, limiting the dataset to the period from March 11, 2020, to December 31, 2022. This inspection will endorse the statistical analysis method that will be useful in summarizing the information in the data set.

In Table 1 statistical summary of the data is presented. From 2020-03-11 to 2022-12-31, for 147 weeks an average of 23417 people were infected with COVID-19 in different counties of Alabama, USA. According to the data, the maximum number of cases is 225876 and the minimum is 2196 registered in counties Jefferson and Greene accordingly. It is worth mentioning that these latter statis-tics also depend on the counties' population. These counts are influenced by both the size and demographic makeup of the populations residing in each area. The relative COVID-19 cases $r_i = Y_i/Pop_i$ provide more specific information according to the counties where Pop_i is the population of county i. Now let us assume that the COVID-19 has uniformly spread throughout the state. Then the number of cases in the state is proportional to the population of the state with the ratio

$$\rho = \sum_{i=1}^{67} Y_i / \sum_{i=1}^{67} pop_i \tag{6}$$

i.e., the rate ρ is calculated by dividing the total number of cases by the state's total population. We have $\rho = 0.32\%$. To address the influence of the counties, the expected numbers of dis- ease risk E1, E67 are determined through standardization. The expected counts Ei for each county i, where i = 1, ..., 67 is computed as:

$$E_i = \rho \times pop_i \tag{7}$$

We normalize the relative cases such that we divide it with ρ , i.e. $r_i/\rho = Y_i/(\rho Pop_i)$, this latter quantity is Y_i/E_i and is called Standard Incidence Rate (SIR) [44]. We concentrate on modelling and investigating the SIR of COVID-19. The SIR is a straight-forward metric used to assess disease risk in specific areas [33, 34]. It is calculated as the ratio between the number of observed cases Yi and the number of expected cases Ei in the ith area,

$$SIR_i = Y_i / E_i \tag{8}$$

Thus, an area with an SIR_i > 0.893 corresponds to a high-risk area as there are more cases observed than expected. On the other hand, an area with an

Table 1. Summary for COVID-19 cases data per county in Alabama State

Min.	1st Qu.	Median	Mean	3rd Qu.	Max.	Var
2194	5634	10357	23417	28833	225876	225876

 $SIR_i < 0.708$ corresponds to a low-risk area. Figure 4 and 5. provides a visual representation of the SIR map. However, the SIR becomes an unreliable measure of disease risk, particularly when dealing with rare diseases or small populations at risk, resulting in small values for the expected number of cases E_i . Due to this instability, researchers often opt for an alternative approach to estimate risk by utilizing model-based methods [11, 13].

To visually represent each group, a custom colour palette was defined. Utilizing the ggplot2 pack- age, we crafted an informative choropleth map, employing distinct colours to distinguish and delineate geographical locations based on their respective value of case groups.

Improved interpretabilitywas achieved by adding labels to the map using the <code>geom_sf_text</code> function. This methodology facilitated the creation of insightful plots, as exemplifiedby **Fig. 3** and **Fig. 4**, offer a comprehensive dataset representation.

Fig. 3a and 3b provide insightful visualizations of the pandemic's impact across diverse counties in Alabama. Each county is represented by a shaded area, with colours indicating the disparity between actual confirmed actual cases and expected cases. The accompanying legend serves as a reference, establishing a connection between colours and specific categories of cases and expected cases. Counties shaded in green, like Choctaw, Washington, Wilcox, and Clay, indicate a "Very

Low" number of expected cases compared to the actual confirmed cases. Conversely, yellow areas, covering counties such as Pickens, Randolph, and Geneva, signify a "Low" number of actual cases compared to the expected ones. White regions, encompassing counties like Chilton, Lee, Coffee, and others, signal a "Medium" difference between observed and expected cases. Counties shaded in light blue, such as Madison, Tuscaloosa, Shelby, and others, demonstrate a "High" difference, while areas shaded in pink, including counties like Jefferson and Mobile, are associated with "Very High" disparities in the numbers of actual confirmed and expected cases.

The visual presentation depicted in **Fig. 4** offers a comprehensive overview, facilitating identification of regions exhibiting heightened SIR on the left **Fig. 4a** and, juxtaposed with the posterior relative risk on the right Fig. 4b, about COVID-19. This aids in grasping the spatial spread of disease prevalence and plays a pivotal role in pinpointing hotspots or areas of particular concern. Specifically, nine counties: -Colbert, Franklin, Morgan, Winston, Cullman, Walker, St. Clair, Clay, and Hale have been classified as hotspots due to their SIR values exceeding 0.893 on the SIR map. Similarly, al-most identical results were achieved using the same classification threshold value, except for two counties Choctaw and Russe which were classified as low-risk counties based on SIR but as high-risk hotspots in the posterior risk maps.

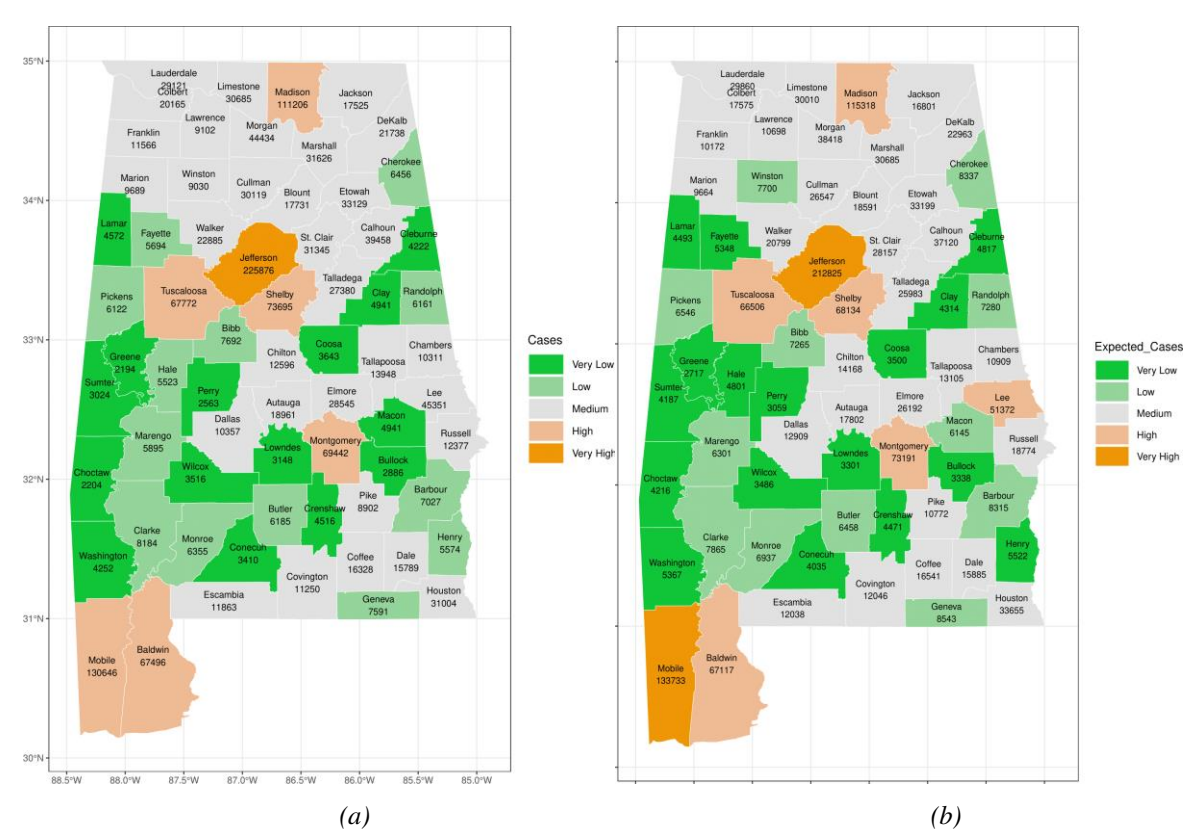


Figure 3. Map of Alabama: Covid-19 Confirmedcases (a) and Expected cases (b) per Counties.

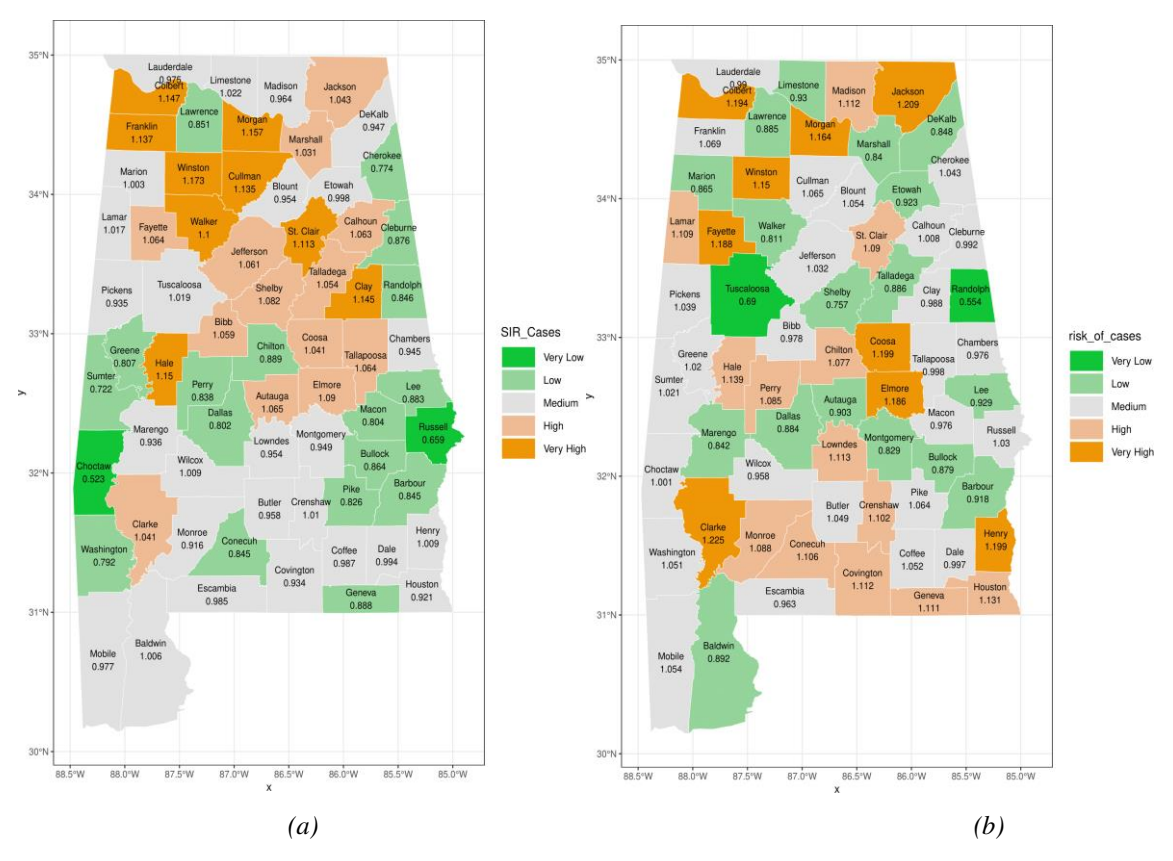


Figure 4. Visualization of SIR (a) and postier risk ξ (b) for cases per Counties, Alabama.

This highlights the effectiveness of utilizing both SIR and posterior relative risk in tandem for dis-ease surveillance and hotspot identification. The SIR values provide insight into the standardized incidence rates, enabling comparisons across regions population considering while differences. Conversely the posterior relative risk offers a nuanced understanding of the risk of disease occurrence in one area compared to a reference group, allowing for a more localized assessment of risk. In this case, the discrepancies between SIR and relative risk classifications for Choctaw and Russe counties underscore the importance of considering multiple metrics for a comprehensive understanding of disease distribution and risk assessment.

1. Model

In epidemiology, disease mapping has a long history, and one of its main objectives is to look into the spatial distribution of disease burden [15, 27]. At the county level, the BYM model [2, 4, 39] was utilized to investigate the geographical

distribution of the SIR of COVID-19 connected to Relative risk It is a widely used spatial model that acknowledges the spatial correlation of data and recognizes that neighbouring areas exhibit greater similarity than distant areas [6, 10, 44, 49].

This model incorporates a spatial random effect that smooths the data based on a neighborhood structure. Additionally, it includes an unstructured exchangeable component that captures uncorrelated noise [34,51]. To visualize and understand the relationships between variables and COVID-19 relative risk, we consider COVID-19 dataset with spatially referenced dataset with spatially referenced observations Yi at location i, and let S be the set of all locations in Alabama state. The Poisson distribution is commonly employed as a standard model for count data [21, 47]. It serves as the foundation for many of the count models utilized by analysts today within a hierarchical Bayesian framework [9, 35]. The Bayesian spatiotemporal model is critical for assessing disease propagation and identifying places with high incidence rates across time and space [25]. This model, which incorporates the susceptibility infection recovery paradigm, enables a complete examination of illness trends within populations. It successfully considers a variety of factors that influence illness prevalence, including physical geographical components such as temperature, rainfall, and air pollution, as well as socioeconomic elements such as economic indicators, healthcare accessibility, demographic characteristics. The applications of Bayesian spatiotemporal models are numerous and important [53]. Firstly, in dis-ease surveillance, these models provide real-time risk assessments and dynamically monitor disease spread. Secondly, they

assist in epidemic forecasting by simulating spatiotemporal disease patterns, enabling accurate predictions and timely interventions. Numerous case studies have validated the effectiveness of these models [42, 43, 45]. The BYM model assumes that the observed counts follow a Poisson distribution:

$$Y_i \sim \text{poisson}(\lambda i)$$
 (9)

where λ_i is the expected rate at location *i*. The key feature of the BYM model is the decomposition of the expected rates $\lambda_i = \rho_i E_i$ where ρ_i corresponds to the relative risk in area *i*. Here E_i denotes the expectation of the number of cases for each area and acts as an offset to the Poisson model. In this case, the linear predictor is defined on the logarithmic scale

$$\eta_i = \log(\rho_i) = a_0 + u_i + v_i \tag{10}$$

such that $\rho_i = exp \ (\alpha + u_i + v_i)$. In this equation α represents the average rate across all areas, u_i is the spatially structured residual, and v_i is an unstructured exchangeable component that is modeled as independent and identically distributed normal variables with zero mean and variance σ^2 . In the BYMmodel, the spatially structured residual, u_i , of (6) is modeled using the intrinsic conditional on neighbors u_{-i} autoregressive (iCAR) specification

$$u_i \mid u_{-i} \sim Normal\left(\mu_i + \sum_{j=1}^n r_{ij}(u_i - u_j), s_i^2\right)$$
 (11)

In the context of equation (6), μ i represents the mean value for area i, and $s2 = \sigma$ 2/Ni corresponds to the variance within the same area. The variance depends on the number of neighbours Ni that an area has, meaning that if an area has a larger number of neighbours, its variance will be smaller [37]. This variance structure acknowledges that when there is a strong spatial correlation, areas with more neighbours contain more information in the data regarding the value of their random effect. The variance parameter σ 2 controls the amount of variation be- tween the spatially structured random effects. The value of ri j represents the spatial proximity between areas and can be computed as:

$$r_{ij} = \begin{cases} 1/N_i, & \text{if areas i and j are neighbours} \\ 0, & \text{otherwise} \end{cases}$$
 (12)

It is important to note that rii is set to 0. County specific relative risks of cases are estimated as $\zeta i = e\alpha + ui + vi$. The above formulae of the BYM model are used for mapping COVID-19 incidences and are implemented using R-INLA see [24, 36, 45].

2. Integrated Nested Laplace Approximation

The INLA is a powerful computational approach designed for approximate Bayesian inference in complex hierarchical models, particularly when dealing with latent Gaussian models [41]. Thecore

idea behind INLA is to use a combination of nested Laplace approximations to efficiently compute posterior distributions without resorting to traditional, often computationally expensive, MarkovChain Monte Carlo (MCMC) methods [17]. INLA has gained popularity due to its ability to handle high-dimensional problems and provide accurate approximations quickly [34, 41]. It is particularly well-suited for spatial spatiotemporal models, allowing for the analysis of complex data structures in fields such as epidemiology, environmental science, and disease mapping. INLA's flexibility and efficiency have made it a valuable tool in various application areas, including risk assessment, ecology, and public health, where researchers of- ten needs to model intricate dependencies and un- certainty in data.

A practical example of INLA's application isin analysing the spread of infectious diseases like COVID-19 [36]. For instance, public health officials seeking to understand the geographic distribution of COVID-19 cases within a state like Alabama might consider factors such as population density, healthcare access, and socioeconomic conditions. By employing the INLA model, they can construct a spatial regression framework that incorporates these variables while accounting for spatial relationships between neighbouring regions.

3. Dataset Analysis

In this study, the BYM model [8] was used to explore the spatial distribution of COVID-19 risk in Alabama. We estimated the relative risk (RR) of COVID-19 incidence for each county in Alabama state and compared it to the SIR and RR, which were used as the baseline reference, and calculated 95% credible intervals (CrI). The RR was significantly higher than 1 when the 95% CrI was over 1. A map of the incidence patterns or probability risk was then generated using the RStudio 2023.06.2 version.

III. RESULTS

This study was initiated to investigate the relative risk of COVID-19 cases in Alabama counties and yields significant findings.

This outcome implies an average decrease of 4.3% in the COVID-19 cases rate across the 67 surveyed counties. The incorporation of a 95% credibility interval enhances precision, supplying a range within which we can confidently assert that the expotentiated intercept's true value exists. The interval, ranging from 0.927 to 0.987, corresponds to a 95% probability that the real impact lies within this bracket. To be more specific, the interval suggests a potential reduction in the COVID-19 cases rate, spanning from 7.3% to 1.3%. In essence, the combined implications of the posterior mean and credibility interval indicate a statistically substantiated average decline in the relative risk of

COVID- 19 across Alabama counties, providing valuable insights for shaping public health decisions and policies. In the risk classification process, it is crucial to prioritize areas for intervention and address heightened morbidity and mortality in future outbreaks by examining the geographic spread of extreme relative risks. To achieve this goal, we utilize a combination of data manipulation and visualization techniques to develop an informative and visually captive risk. To pinpoint regions with increased, occurrence of a specific phenomenon, we adopt criteria rooted in exceedance probability. The probability that the relative risk of area i is higher than a value c can be written as P ($\rho i > c$). This probability can be calculated by subtracting P (pi c) to 1 as follows:

$$P(\rho_i > c) = 1 - P(\rho_i \le c) \tag{13}$$

To compute the probability $P(\rho | c)$ in R-INLA, use the inla.pmarginal() function with ρi 's marginal distribution and c as the threshold value. The spatial exceeding probability is calculated using the posterior distribution of the relative risk. This analytical metric gives useful information about the likelihood of the calculated posterior relative risk exceeding a predefined threshold value inside a specific area.

Fig. 5 illustrates the COVID-19 county SIR (Standard Incidence Rate) trends about Alabama mortality rates from March 11, 2020, to December 31, 2022. This graphic has five unique color-coded groups. Some Alabama counties, including Walker,

Etowah, Hale, Lowndes, and Crenshaw, have considerably higher relative risks of COVID-19 incidence and mortality rates, above the baseline reference of > 1, placing them in the orange category. In contrast, about four counties, including Madison, Shelby, Lee, and Russell, had much reduced relative risks in both COVID-19 instances and mortality rates and so were allocated to the green group. It's worth noting that the remaining counties typically fell somewhere in between these extremes, as indicated by the plot's legendary different colour ranges. Identifying hotspots or regions of danger is crucial for evidence-based policymaking since these sites act as epicentres, playing an important role in the spread of phenomena, such as diseases or other occurrences.

Fig. 6 presents hotspots with posterior probability $P(e^{oi} > 1 y)$ of relative risk of COVID-19 cases versus deaths. The figure shows that the bulk of relative cases hotspots emerged in the Northern and central counties of Alabama, including Lauderdale, Madison, Jackson, Franklin, Jefferson, and Shelby, to mention a few.

Furthermore, certain northern and central counties nearby (though not neighboring) continued to be identified as hotspots for death risk, albeit in fewer numbers. These counties include Pickens, Greene, Lawrence, Etowah, Calhoun, Covington, among others. **Fig. 6** shows the discrepancy between counties where the relative risk and likelihood of death are greater than one.

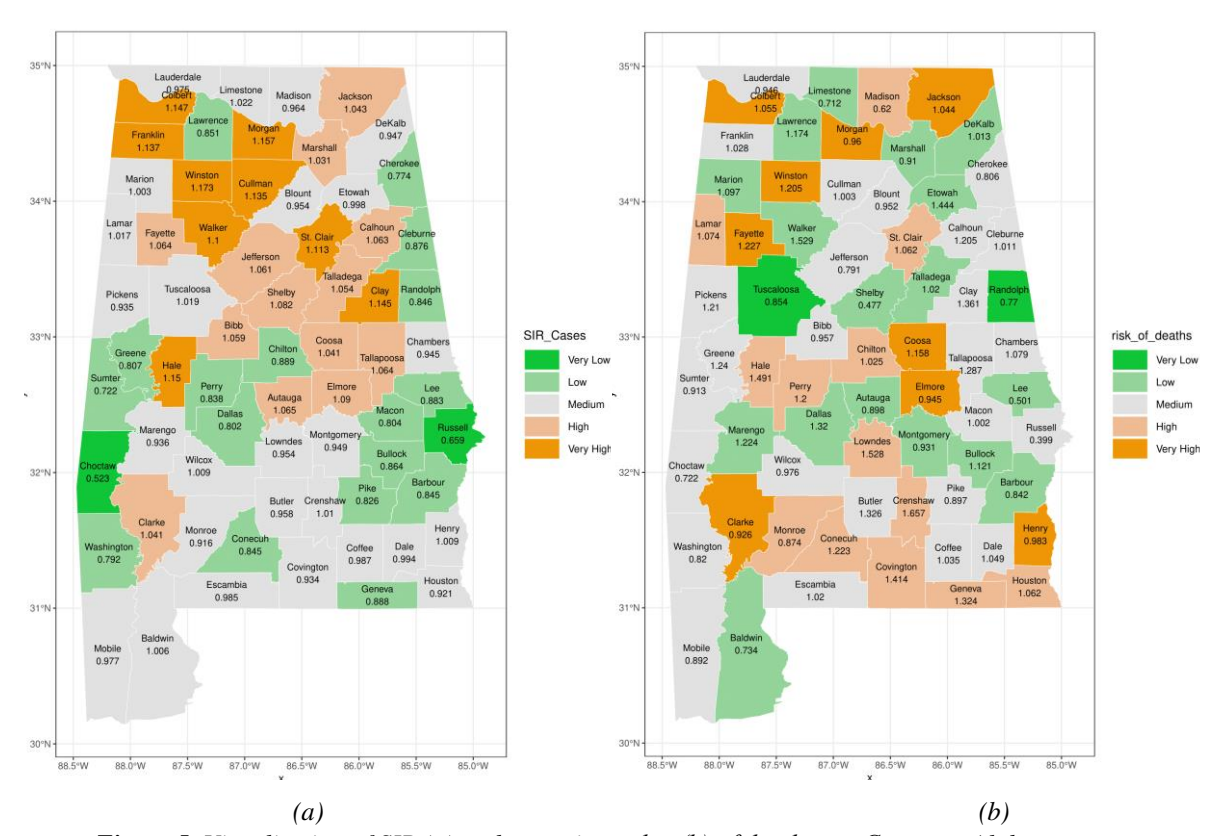


Figure 5. Visualization of SIR (a) and posterior risk ρ (b) of deaths per Counties, Alabama.

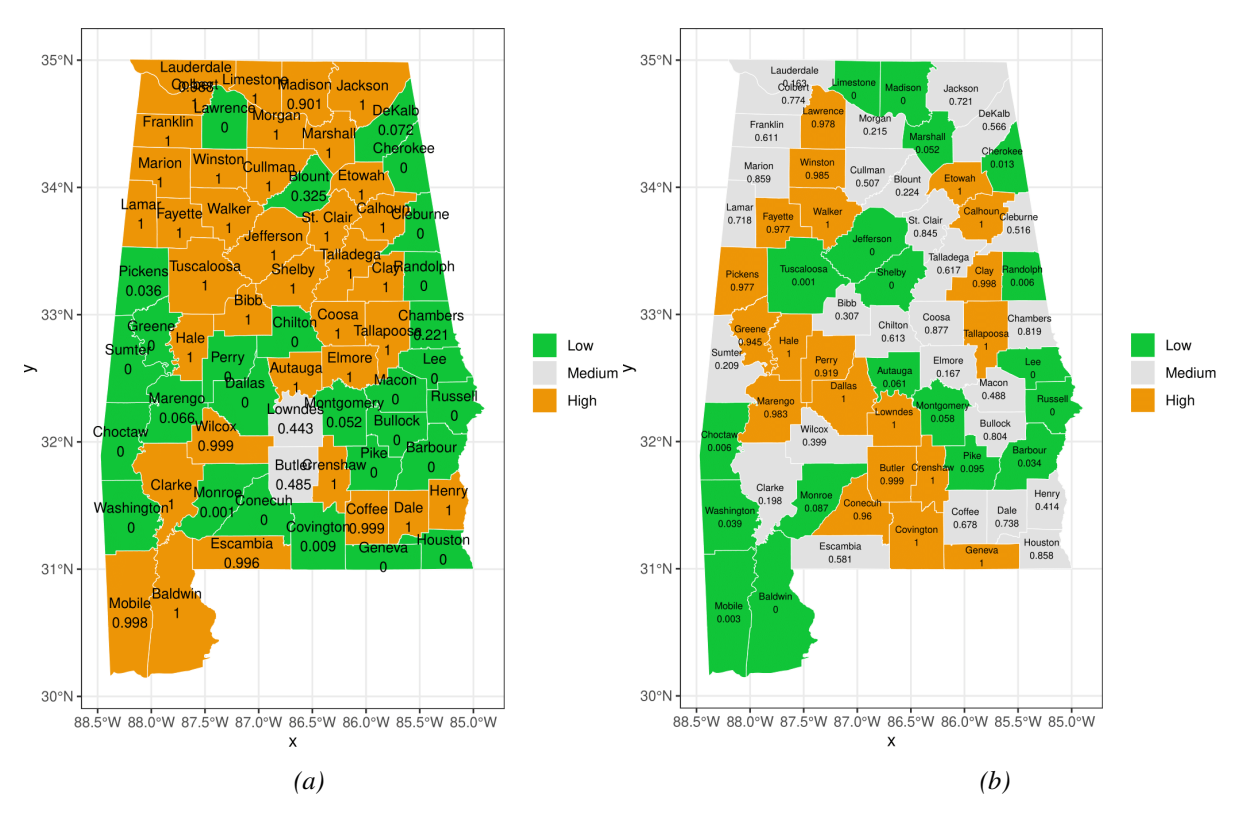


Figure 6. Visualization of posterior probability $P(e^{p_i} > 1 \text{ y})$ of relative risks, per Counties, Alabama.

Using relative risk as an illustration, **Fig. 6a** and **6b** demonstrates that the county at the center has a relative risk surpassing one (depicted in orange), yet it is not classed as a hotspot (marked by a green hue). This is because its exceedance probability is less than 0.398, hence it does not qualify as a hotspot.

IV. DISCUSSION

The fundamental goal of disease mapping is the identification of high-risk locations, which is essential for formulating effective public health strategies. The consequences of a disease mapping model inaccurately predicting cases or deaths in these high-risk regions could lead to misaligned resource allocation decisions that do not address the actual health needs. Additionally, understanding areas with distinctly low risk is crucial, not only for optimizing resource allocation but also for discerning environments that foster a reduction in health risks.

This study was centred on spatial data processing for statistical modelling and visualization, specifically utilizing the BYM model in R-INLA package for COVID-19 in the case of Alabama. We focused on estimating the relative risk of COVID-19 across 67 counties, underscoring the critical importance of accurate disease mapping in public health endeavours. The results of our analysis, particularly the posterior mean of the exponentiated intercept, revealing a substantial 4.3% decrease in the COVID-19 case rate, offer indispensable in-

sights. The 95% credibility interval of 0.927 to 0.987 linked with our findings enhances the robust-ness of our estimations, presenting a nuanced range of 7.3% to 1.3%.

V. CONCLUSION

In conclusion, this study leveraged spatial data processing, Bayesian analysis, and advanced statistical modeling, specifically employing the INLA model, to investigate the relative risk of COVID-19 cases across Alabama counties. The calculated posterior mean of the exponentiated intercept α value for relative risk indicated a statistically significant average decrease of 4.3% in the COVID-19 risk rate. The incorporation of a 95% credibility interval (0.927 to 0.987) added precisionto the findings, providing a range within which thetrue value of the exponentiated intercept is likely to exist, suggesting a potential reduction in the COVID-19 cases rate ranging from 7.3% to 1.3%. It is worth noting that the posterior mean of the exponentiated intercept $\alpha = 1.1126$ with credibility interval (1.0387 to 1.1903). This implies that $\alpha > 1$ is significant, contrary to the cases when it is smaller than 1.

These results hold substantial implications for public health decision-making, guiding policymakers in prioritizing areas for intervention based on the relative risk distribution. The classification of risk, depicted in the visual representation of COVID-19 relative risk patterns

across Alabama counties from March 11, 2020, to December 31, 2022, revealed notable disparities. Counties such as Colbert, Franklin, Morgan, Winston, Cullman, Walker, St. Clair, Clay, and Hale exhibited significantly higher relative risks, categorizing them in the orange color group. In contrast, several counties witha relative risk range below 0.398 were designated as green, indicating lower risk. Notably, counties like Lowndes and Butler fell within the moderate risk range (0.398 to 0.796), as depicted by the white hue.

This comprehensive analysis, combining statistical insights with visual representations, contributes valuable information for proactive public health measures. By identifying regions with elevated risk, authorities can strategically allocate resources, implement targeted interventions, and mitigate the im-pact of future epidemics. The integration of spatial data processing and visualization techniques enhances our understanding of the geographic distribution of relative risk, fostering informed decision- making for effective public health management.

NOMENCLATURE

 ρ The autocorrelation

BYM Besag, York, and Mollié

E Expected value of a random variable, inunite of a random variable.

GIS Geographical Information Systems

POP Population of county.

RR Relative Risk.

REFERENCES

- [1] T. Alamo D. G. Reina, P. Millán. Data-driven methods to monitor, model, forecast and control COVID-19 pandemic: Leveraging data science, epidemiology and control theory. arXiv preprint arXiv: 2006.01731 (2020). https://doi.org/10.1016/j.coi.2020.09.011
- [2] M. A. S. Alhdiri N. A. Samat, Z. Mohamed. Disease mapping for stomach cancer in libya based on besag-york-mollié (bym) model. Asian Pacific Journal of Cancer Prevention: APJCP 18 (6) (2017) 1479. https://doi.org/10.1007/s11356-022-23319-6
- [3] M. P. Armstrong G. Rushton, D. L. Zimmerman. Geographically masking health data to preserve confidentiality. Statistics in medicine 18 (5) (1999) pp. 497–525. https://doi.org/10.1002/(SICI)1097-0258(19990315)18:5
- [4] J. Besag J. York, A. Mollié. Bayesian image restoration, with two applications in spatial statis-tics. Annals of the institute of statistical mathematics 43 (1991) pp. 1–20. https://doi.org/10.1007/BF00058655

SIR Standardized Incidence Rate.

ACKNOWLEDGEMENT

This research by Gy. Terdik was supported by the project TKP2021-NKTA of the University of Debrecen, Hungary. Project no. TKP2021-NKTA-34 has been implemented with support from the Ministry of Culture and Innovation of Hungaryfrom the National Research, Development and Innovation Fund. financed under the TKP2021-NKTA funding scheme.

AUTHOR CONTRIBUTIONS

- **A. D. Getachew:** Writing the manuscript, Writing thecode, and theoretical analysis.
- **B. Gy. Terdik:** Conceptualization, writing the code, Review and editing. Supervision.

DISCLOSURE STATEMENT

The authors declare that they have no known competing financial interests or personal relationships that could have appeared to influence the work reported in this paper.

ORCID

- **D.Getachew** http://orcid.org/0000-0001-7547-943x
- **G. Terdik** http://orcid.org/0000-0002-9663-6892
- [5] M. Blangiardo, M. Cameletti. Spatial and spatio-temporal Bayesian models with R-INLA (2015). John Wiley & Sons.
- [6] M. Blangiardo M. Cameletti G. Baio, H. Rue. Spatial and spatio-temporal models with rinla.Spatial and spatio-temporal epidemiology 4 (2013) pp. 33–49. https://doi.org/10.1016/j.sste.2012.12.001
- [7] P. J. Brantingham. Crime diversity. Criminology 54 (4) (2016) pp. 553–586. https://doi.org/https://doi.org/10.1111/doi:1745-9125.12116.
- [8] M. J. Breslow, O. Badawi. Severity scoring in the critically iii: Part 2: Maximizing value from outcome prediction scoring systems. Chest 141 (2) (2012) pp. 518–527. https://doi.org/10.1378/chest.11-0331
- [9] A. C. Cameron, P. K. Trivedi. Regression analysis of count data (2013). Number 53. Cam- bridge university press.
- [10] J. Chen J. J. Song, J. D. Stamey. A Bayesian hierarchical spatial model to correct for misreporting in count data: application to state-levelCOVID-19 data in the United States. International Journal of Environmental

ns: 140

- Research and PublicHealth 19 (6) (2022) 3327. https://doi.org/10.3390/ijerph19063327
- [11] J. T. Chen. 11 multilevel and hierarchical models for disease mapping. Geographic health data: Fundamental techniques for analysis (2013), pages183. https://doi.org/10.1079/9781780640891.0183
- [12] E. Clement. Small area estimation with application to disease mapping. International Journal of Probability and Statistics 3 (1) (2014) pp. 15–22. https://doi.org/10.5923/j.ijps.20140301.03
- [13] A. Comunian R. Gaburro, M. Giudici. Inversion of a sir-based model: A critical analysis about the application to covid-19 epidemic. Physica D:Nonlinear Phenomena 413 (2020) 132674.
 - https://doi.org/10.1016/j.cossms.2021.100411
- [14] E. Cuevas. An agent-based model to evaluate the COVID-19 transmission risks in facilities. Computers in Biology and Medicine 121 (2020) 103827.

 https://doi.org/10.1016/j.compbiomed.2020.10
 3827
- [15] P. Elliott, D. Wartenberg. Spatial epidemiology: current approaches and future challenges. Environmental health perspectives 112 (9) (2004) pp. 998–1006. https://doi.org/10.1093/ije/dyz047
- [16] I. Franch-Pardo B. M. Napoletano F. Rosete-Verges, L. Billa. Spatial analysis and gis in thestudy of COVID-19. a review. Science of the total environment 739 (2020) 140033. https://doi.org/10.1016/j.scitotenv.2020.14003
- [17] V. Gómez-Rubio, F. Palm Perales. Multivariate posterior inference for spatial models with the integrated nested Laplace approximation. Journal of the Royal Statistical Society Series C: Ap- plied Statistics 68 (1) (2019) pp. 199–215. https://doi.org/10.1111/rssc.12292
- [18] G. Grekousis Z. Feng I. Marakakis Y. Lu, R. Wang. Ranking the importance of demographic, socioeconomic, and underlying health factors on us COVID-19 deaths: A geographical random forest approach. Health & Place 74 (2022) 102744. https://doi.org/10.1016/j.healthplace.2022.102
- [19] R. P. Haining. Spatial data analysis: theoryand practice (2003). Cambridge university press.
- [20] A. Jalilian, J. Mateu. A hierarchical spatio temporal model to analyse relative risk variations of COVID-19: a focus on Spain, Italy and Germany. Stochastic Environmental Research and Risk Assessment 35 (2021) pp. 797–812.
- [21] H. Joe, R. Zhu. Generalized poison distribution: the property of mixture of

- poison and comparison with negative binomial distribution. Biometrical Journal: Journal of Mathematical Methods in Biosciences 47 (2) (2005) pp. 219–229. https://doi.org/10.1002/bimj.200410102Citatio
- [22] M. R. Karim. Bayesian hierarchical spatial modeling of COVID-19 cases in bangladesh. An- nals of Data Science (2023) pp. 1–27. https://doi.org/10.1007/s40745-022-00381-1
- [23] M. U. Kraemer S. I. Hay D. M. Pigott D. L. Smith G. W. Wint, N. Golding. Progress and chal-lenges in infectious disease cartography. Trends inparasitology 32 (1) (2016) pp. 19–29. https://doi.org/10.1016/j.pt.2015.09.006
- [24] E. Krainski V. Gómez-Rubio H. Bakka A. Lenzi D. Castro-Camilo D. Simpson F. Lind- gren, H. Rue. Advanced spatial modeling with stochastic partial differential equations using R and INLA (2018). Chapman and Hall/CRC.
- [25] A. Lal J. Marshall J. Benschop A. Brock S. Hales M. G. Baker, N. P. French. A Bayesian spatio-temporal framework to identify outbreaks and examine environmental and social risk factors for infectious diseases monitored by routine surveillance. Spatial and spatio-temporal epidemi-ology 25 (2018) pp. 39–48.
- [26] K. Lancaster T. Rhodes, M. Rosengarten. Making evidence and policy in public health emergencies: lessons from COVID-19 for adap- tive evidence-making and intervention. Evidence & policy 16 (3) (2020) pp. 477–490. https://doi.org/10.1332/174426420X15913559 981103
- [27] A. B. Lawson. Bayesian disease mapping: hierarchical modeling in spatial epidemiology (2018). Chapman and Hall/CRC.
- [28] P. Legendre. Spatial autocorrelation: trouble or new paradigm? Ecology 74 (6) (1993) pp. 1659–1673. https://doi.org/10.2307/1939924
- [29] J. W. Lichstein T. R. Simons S. A. Shriner, K. E. Franzreb. Spatial autocorrelation and autoregressive models in ecology. Ecological monographs 72 (3) (2002) pp. 445–463. https://doi.org/10.1890/0012-9615(2002)072[0445:SAAAMI]2.0.CO;2
- [30] J. Ma H. Zhu P. Li C. Liu F. Li Z. LuoM. Zhang, L. Li. Spatial patterns of the spread of COVID-19 in singapore and the influencing factors. ISPRS International Journal of Geo- Information 11 (3) (2022) 152. https://doi.org/10.3390/ijgi11030152
- [31] A. Maiti Q. Zhang S. Sannigrahi S. Pra-manik S. Chakraborti A. Cerda, F. Pilla. Ex-ploring spatiotemporal effects of the driving fac-tors on COVID-19 incidences in the contiguous

- united states. Sustainable cities and society 68 (2021) 102784.
- https://doi.org/10.1016/j.scs.2021.102784
- [32] T. J. Mason. Atlas of Cancer Mortality for US counties, 1950-1969 (1975). US Department of Health, Education, and Welfare, Public Health Service.
- [33] J. C. Miller, E. M. Volz. Incorporating disease and population structure into models of sir disease in contact networks. PLOS ONE 8 (8) (2013) e69162. https://doi.org/10.1371/journal.pone.0069162
- [34] P. Moraga. Geospatial health data: Modeling and visualization with R-INLA and shiny (2019). Chapman and Hall/CRC.
- [35] A. K. Muoka O. O. Ngesa, A. G. Waititu. Statistical models for count data. Science Jour-nal of Applied Mathematics and Statistics 4 (6) (2016) pp. 256–262. https://doi.org/10.11648/j.sjams.20160406.12
- [36] N. Nazia Z. A. Butt M. L. Bedard W.-C. Tang H. Sehar, J. Law. Methods used in the spatial and spatiotemporal analysis of COVID-19 a systematic review. epidemi- ology: International Jour- nal of Environmental Research and Public Health 19 (14) (2022)
 - https://doi.org/10.3390/ijerph19148267
- [37] K. W. Pettis T. A. Bailey A. K. Jain, R. C. Dubes. An intrinsic dimensionality estimator from near-neighbor information. Transactions onpattern analysis and machine intelligence 1 (1979) pp. 25-37.
- [38] P. Puvanachandra C. Hoe T. Özkan, T. Lajunen. Burden of road traffic injuries in turkey. Traffic injury prevention 13 (1) (2012) pp. 64–
 - https://doi.org/15389588.2011.633135
- [39] A. Riebler S. H. Sørbye D. Simpson, H. Rue. An intuitive bayesian spatial model for disease mapping that accounts for scaling. Statistical methods in medical research 25 (4) (2016) pp. 1145-1165.
 - https://doi.org/10.1016/j.sste.2016.10.014
- [40] A. D. Roux C. I. Kiefe D. R. Jacobs Jr M. Haan S. A. Jackson F. J. Nieto C. C. Paton, R. Schulz. Area characteristics and individual-level socioeconomic position indicators population-based three epidemiologic studies. Annals epidemiology 11 (6) (2001) pp. 395-405. https://doi.org/10.1016/S1047-2797(01)00221-6
- [41] H. Rue S. Martino, N. Chopin. Approximate Bayesian inference for latent gaussian models by using integrated nested Laplace approximations. Journal of the Royal Statistical Society Series B:Statistical Methodology 71 (2) (2009) pp. 319–392.

- https://doi.org/10.1111/j.1467-9868.2008.00700.x
- [42] P. Saavedra A. Santana L. Bello J.-M. Pacheco, E. Sanjuán. A bayesian spatiotemporalanalysis of mortality rates in spain: application to the covid-19 2020 outbreak. Population Health Metrics 19 (1) (2021) 27. https://doi.org/10.1186/s12963-021-00259-y
- [43] A. K. Sahu V. T. Amritha Nand R. Mathew P. Aggarwal J. Nayer, S. Bhoi. Covid-19 in health care workers-a systematic review and meta- analysis. The American Journal of EmergencyMedicine 38 (9) (2020) pp. 1727
 - https://doi.org/10.1016/j.ajem.2020.05.113
- [44] S. K. Sahu, D. Böhning. Bayesian spatiotemporal joint disease mapping of COVID-19 cases and deaths in local authorities of england. Spatial Statistics 49 (2022) 100519. https://doi.org/10.1007/s11356-021-12925-2
- [45] P. Satorra, C. Tebé. Bayesian spatio-temporal analysis of the covid-19 pandemic in Catalonia Scientific Reports 14 (1) (2024) 4220.
 - https://doi.org/10.1007/s11749-021-00769-4
- [46] O. Schabenberger, C. A. Gotway. Statistical methods for spatial data analysis (2017). Chapmanand Hall/CRC.
- [47] K. F. Sellers S. Borle, G. Shmueli. The compoison model for count data: a survey of methods and applications. Applied Stochastic Models in Business and Industry 28 (2) (2012) pp. 104-116.
- [48] S. Sisman, A. C. Aydinoglu. A modelling approach with geographically weighted regressionmethods for determining geographic variation and influencing factors in housing price: A case inistanbul. Land use policy 119 (2022) 106183. https://doi.org/10.1016/j.landusepol.2022.1061
- [49] R. J. Thomas. Female consumption and evaluation of traditionally male orientated products: aself-monitoring perspective (2010). University of South Wales (United Kingdom).

83

- [50] P. H. Verburg K. Kok R. G. Pontius Jr, A. Veldkamp. Modelling land-use and land-cover change. In: Land-use and land-cover change: local processes and global impacts, pp. 117-135 Springer (2006).
- [51] L. A. Waller L. Zhu C. A. Gotway D. M. Gorman, P. J. Gruenewald. Quantifying geographic variations in associations between alcohol distribution and violence: a comparison of geographically weighted regression and spatially varying coefficient models. Stochastic Environmental Re-search and Risk Assessment 21 (2007) pp. 573–588. https://doi.org/10.1007/s00477-007-0139-9

- [52] S. Wang X. Yang L. Li P. Nadler R. Arcucci Y. Huang Z. Teng, Y. Guo. A Bayesian updating scheme for pandemics: estimating the infection dynamics of COVID-19. IEEE Computational Intelligence Magazine 15 (4) (2020) pp. 23–33. https://doi.org/10.1016/j.jbi.2020.103347
- [53] Y. Wang X. Chen, F. Xue. A review of Bayesian spatiotemporal models in spatial
- epidemiology. ISPRS International Journal of Geo-Information 13 (3) (2024) 97. https://doi.org/10.3390/ijgi13030097
- [54] A. Woo ditch N. J. Johnson R. Solymosi J. Medina Ariza, S. Langton. Getting to know your data. In: A Beginner's Guide to Statistics for Criminology and Criminal Justice Using R, pp. 21–38. Springer (2021).



This article is an open access article distributed under the terms and conditions of the Creative Commons Attribution Non-commercial (CC BY-NC 4.0) license.



ACTA TECHNICA JAURINENSIS

Vol. 17, No. 3, pp. 143-151, 2024 10.14513/actatechjaur.00727



Mini Review

Review on Coordination of Time Overcurrent Relays in Electrical Distribution Network

Godfrey Mhagama^{1,*}, Ndyetabura Y. Hamisi¹, Shililiandumi Naiman²

¹Department of Computer Science and Engineering, College of Information and Communication Technologies University of Dar es Salaam, P.O. Box 33335, Dar es Salaam, Tanzania

²Department of Electronics and Telecommunication Engineering, College of Information and Communication Technologies, University of Dar es Salaam, P.O. Box 33335, Dar es Salaam, Tanzania *e-mail: eng.godfreymhagama@gmail.com

Abstract:

Integration of distributed generators in micro grid causes bidirectional current flow as a result of the need for readjustment of the setting of the overcurrent protective relays in the electrical network. Adaptive coordination is one of the solutions that adjust the setting of protective relays according to the dynamics of the distribution network. Various algorithms had been reported on the adaptive coordination of time overcurrent relays. This paper reports a survey about the coordination of time overcurrent relays in micro grid electrical distribution network. The review found that there is limited research on distributed control rules of the multi agent coordination of protection relays. Furthermore, it was found that the trend of coordination algorithms focused on the nature inspired algorithms.

Keywords: protection; relay; coordination; operating time; distribution network; algorithm

I. Introduction

distribution electrical encompasses the electrical conductors transporting electrical energy from sources to sinks. In this context the sources are represented by the electrical generators and substations, and the sinks are represented the electrical loads. The electrical distribution networks are geographically distributed in a non-uniform arrangement based on the settlements of the societies who are the users of the electrical energy. Load current in electrical distribution networks varies close to the setting of protective relays the condition that causes false tripping commands of relays. In the legacy electrical distribution network the source of power is the utility source, however the higher demand on power and reliability issues have brought the need for installation of distributed generators in the electrical distribution network near the load centres. The modern electrical distribution network has different sources of power including solar power, distributed generators, and energy storage systems; all these are integrated in the distribution networks to supply power required for the loads. Along the distribution networks, there are protection devices to control the electrical power. Relays are among the protection

devices that sense and send tripping commands to the circuit breakers on the occurrence of a fault. As the network expands the number of relavs increases and their accuracy of operation depends on coordination. Coordination of relays in the electrical distribution network is among the classical protection problems with the objective to set the operating time for the relays as accurately as possible to allow the proper operation of the protection system when a fault occurs. The coordination of relays in electrical distribution networks is affected by the operating level of the electrical network, dynamics of the electrical current in the system, characteristics of protection devices, the type of the protection scheme, and the type of technology used. The operation of the power system protection devices involves current, and time. This approach had been a normal practice in the power system protection industry and its implementation had been revealed in transmission lines and substations. The need for installation of protection devices in the distribution networks brings attention about the parameters of the agents for protection.

Introduction of the overcurrent relays in power systems dates back in 1905 according to ABB products [1]. The coordination of overcurrent relays involves optimizing the setting of individual relay and was first reported in 1988 [2]. The author in [2] used the minimax optimisation approach. Since the year 2012 various articles about coordination of the overcurrent relays had been published. In 2012 the author in[3] reported the use of Seeker Algorithm for coordination of overcurrent relays. One of the drawbacks of the Seeker Algorithm is the high computational time requirement. In 2014 the Table based Algorithm was reported for use in inverse time overcurrent relay [4]. The disadvantage of the Table based Algorithm is the requirement for high memory resource but its advantage is high speed of performance [4]. The use of hybrid particle swarm optimizationgravitational search algorithm for overcurrent relay coordination was reported in 2016[5]. The metaheuristic algorithm was reported in 2017 for coordination of overcurrent relays Advantages of metaheuristic algorithm is smaller processing time [6]. The use of metaheuristic algorithm was also reported in 2018 for coordination of overcurrent relays [7]. The hybrid Whale Optimisation algorithm and Grey Wolf optimizer algorithm was reported in 2019 for coordination of overcurrent relays [8]. The enhanced differential evolution multi-objective algorithm was reported in 2019 for coordination of overcurrent relays [9]. The Teaching Learning Based Optimisation algorithm was reported in 2021 for coordination of overcurrent relays [10]. Advantage of the Teaching Learning Based Optimisation algorithm includes computational efforts for problems of high dimensionality. According to the trend of publication, the research on new algorithms comes into application from time to time but no superior algorithms for every type of the problem [11]. The direction of research for optimisation algorithms shows that the nature inspired algorithms are among the state of the art methods for optimization [12].

With advancement of technology, the coordination of relays can be implemented either with communication or without communication. The coordination that is associated with communication builds up both the physical electrical connections and the communication between the relays. The combination of protection system and telecommunication results in teleprotection. Other literatures describe as the communication assisted adaptive protection. In teleprotection the relays are connected by the telecommunication network as shown in Fig.1.

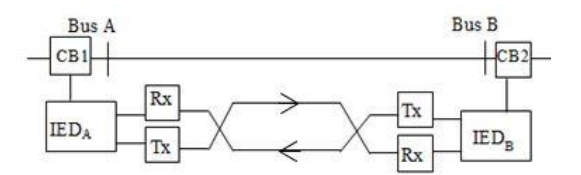


Figure 1. Teleprotection Layout

From Fig.1, the CB represents circuit breaker, IED represent the Intelligent Electronic Device, Tx represent transmitter, Rx represent the Receiver. The technology evolution of relays changed from static relays in 1974 to numerical relays in 1999 [1]. By the year 2000 the relays technology had advanced to digital relays and IEDs with high selectivity. Coordination of protective relays especially on overcurrent relays had been published by various researchers reporting different methods and techniques to improve the coordination of relays. There had been various review articles on the coordination of relays. A review of the protection challenges such as bidirectional fault current, and various levels of fault current under different operating conditions had been reported in [13]. The need for different settings for the protection devices placed along the network for micro grid had been addressed by the use of the logic selectivity method [14]. The Evolutionary Particle Swarm Optimisation algorithms based on Fuzzy systems had been used to address the challenges of designing robust and flexible power systems under a variety of operating conditions [15]. The method of Micro grid Central Controller reconfiguration algorithm based had been reported to address the change of topology of micro grids and dynamics in fault current magnitude [16]. Numerical optimisation-based solution to directional overcurrent relay coordination had been solved by Integer Linear Programming Linearization of variables using disjunctive inequalities [17]. First Depth Search and Variable Neighborhood Search methods were applied to address the problem of difficulty in the determination of an optimal setting for relay coordination [18]. The need to have new protection schemes for modern power system had been addressed in [13]. Researches show that there are advantages of using teleprotection in coordination of relays [15-16, 19-20].

With the increasing complexity of modern distribution systems, the utilization of multi-agent coordination mechanisms has gained attention to enhance the performance and efficiency of teleprotection relays. Multi agent approach for coordination of relays had been reported in different articles [21-25]. Adaptive coordination has been reported in various articles about optimal coordination of overcurrent relays with the aim of overcurrent relays to self-adjust the setting of the

protection when the operating limits change [24], [26-30]. In this paper there are four next sections. Section two contains the method that was used in the systematic review. Section three comprises of result. Section four is the section with the discussion. Section five provides conclusion from the review study.

II. METHODOLOGY

A systematic literature review was conducted to identify relevant research articles, conference papers, and technical reports. The selected research articles were those related to coordination of overcurrent relays and the use of multi-agent coordination in teleprotection relay systems. The selected studies were analyzed and synthesized to provide an overview of the current state of research in this area. The works of literature on the coordination of relays had been synthesized by a systematic review that employed the evidence-based practice methodology [31, 32], and used the results from various studies on the coordination of relays. Steps that were involved to carry out the systematic identification, review included; selection, assessment, extraction and synthesis. Selection involved screening the articles, extraction, and synthesis. The screening process was achieved by the use of the exclusion and inclusion criteria. To get an understanding of the research about coordination of relays the research questions were involved including; Where do the articles on coordination of relays in electrical networks are published? What types of articles had been published on the coordination of relays in electrical distribution networks? Which themes had been covered in the published literature on the coordination of relays? What method had been used in the published articles on the coordination of relays in electrical distribution networks?

Searching of articles on the topic of protection and coordination of relays specified the publication time from January 2013 to December 2022. The articles were accessed from various online resources. The online resources included but were not limited to; google scholar, IEEE, web of science, Researchgate, arXiv, vendors of equipment, proceedings, and published standards. The inclusion and exclusion criteria were applied to screen the articles for further detailed review. The search involved the search theme and the search strategy (Table 1.). Some of the search theme included; coordination, adaptive, overcurrent relay. Some of the search strategies included: 'relay' OR 'IED' AND 'coordination' AND 'adaptive' 'protection' AND 'overcurrent' AND 'relay' AND 'coordination' AND 'AC' AND 'microgrid'. 'relay' AND 'coordination' OR 'multiagent' OR 'multiagent'.

Inclusion criteria included analysis based on the theoretical papers, working paper, quantitative and qualitative empirical studies. There were many criteria for inclusion, to mention few criteria; the distribution network was also inclusion criteria, the microgrid was one of the inclusion criteria, and also the overcurrent protection was the inclusion criteria. Exclusion criteria included analysis based on the publication year beyond the specified, electrical transmission network, non-relevance of the contents of the article, and the article with language other than English. The searched articles were stored in the computer folder and the computer folder was added to the Mendeley Desktop [33]. The file name of the article had to have the author's name, title of the article, journal name and year of publication.

Table 1. Steps

Step	Output
Searching	Total number of articles
Screening	Abstract and title
Eligibility	Full text review
<i>c</i> ,	Quantitative/Qualitative
Detailed analysis	Synthesis

The published articles about coordination of relays that involved communication were further analysed in detail with the focus on the differential protection and overcurrent protection to obtain the extent of the application of the protection schemes. The methods for differential protection work on the principle of difference of the electrical current between two points. The sampled value packets loss was used for transformer differential protection, time-frequency transform-based differential protection had been reported for use in micro grid, also the Intelligent Differential Microgrid Protection Scheme had been reported. Other relevant published articles included the variable tripping time differential protection for micro grid, Feature Cosine and Differential Scheme for Micro grid, secure communication for line current differential protection systems over packet switched networks and Packet-Based Networks for Current Differential Protection Application. The overcurrent protection schemes work on the principle of pickup current setting of the protection device considering the constraint of the coordination time interval.

In order to illustrate the involvement of the algorithms, this study adopted the three bus electrical network shown in **Fig.2** [34, 35]. The set of data used in this study was as those in [35]. In this review the Genetic Algorithm (GA) was used to optimise the TMS of the backup relays and then the optimised TMS was used to compute the corresponding operating time. The results obtained by using GA were compared to the result from the literature [35].

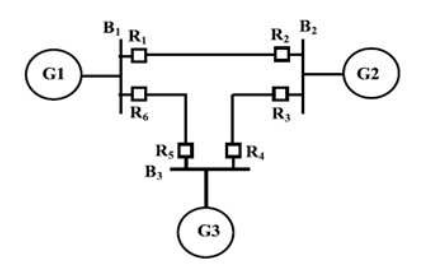


Figure 2. Three bus network

The fault currents for the three bus network were as shown in **Table 2** [35].

Table 2: Fault currents

Table 2: Fault currents				
Primary		Backup		
Relay		Relay		
Fault			Fault	
current		current		
	(A)		(A)	
R1	2075.0	R5	400.7	
R2	1621.7	R4	700.64	
R3	1779.6	R1	760.17	
R4	1911.5	R6	622.65	
R5	1588.5	R3	558.13	
R6	1855.4	R2	380.70	

Equation (1) was the time current curve.

$$t = TMS\left(\frac{\beta}{PSM^{\alpha}-1}\right) \tag{1}$$

Equation (2) was the objective function.

$$F(t) = \sum_{i=1}^{N} t_i$$
 (2)

Equation (3) was the constraint.

$$t_i^{\text{backup}} - t_i^{\text{primary}} \ge \text{CTI}$$
 (3)

where:

 $t_{\rm i}$ is the operating time of individual relay in seconds.

F(t) is the total operating time of all relays in the network.

 $t_i^{primary}$ is the operating time of the primary relay t_i^{backup} is the operating time of the backup relay CTI is the coordination time interval.

N was the number of relays.

The values of α and β were 0.02 and 0.14 respectively.

Equation (4) was used to compute the Plug Setting Multiplier(PSM).

$$PSM = \frac{CTRxFault current}{Plug setting}$$
 (4)

The CTR was the current transformer ratio. The GA was implemented by python and the steps were:

- i. Start:
- ii. Initialise the parameters;
- iii. Initialise objective function;
- iv. Extract one parent in each iteration;
- v. Carry out crossover and mutation;
- vi. Return best result.

The lower and upper limits of the TMS were 0.1000 and 0.3000 respectively.

III. RESULT

Various articles used different types of networks for testing the proposed methods and algorithms. The operating time of the relay is the dependent variable that depends on the value of the load current and pick up current. The value of fault current was less than 12 kA and the range of pickup current was between 0.5 A to 1.15 A [36, 37]. Based on the time current curve characteristics, the published articles that mentioned the type of curve either used the IEC 60255-3 or IEEE C37.112. However, some articles did not specify the reference type of the time current curve. There was high number of articles related with optimisation algorithms. The review identified several studies that explored the integration of multi-agent coordination to enhance teleprotection relay systems. These studies use of reported that the agents communication-based protection demonstrated improvements in fault detection accuracy, reduction in communication delays, and increased reliability through collaborative decision-making among teleprotection relays.

The articles focused on the areas such as coordination, algorithm, teleprotection, agent, and communication as shown in **Fig. 3. Table 3.** shows some of the algorithms that were used in the recent articles concerning the coordination of relays. **Fig. 4.** was the result for the extent of the use of the differential protection and overcurrent protection.

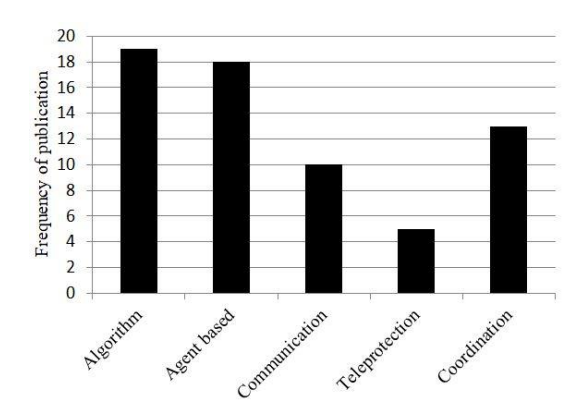


Figure 3. Focus area of the published articles

Table	3: Result	for backu _l	p relays
	T		TT1 :

	Literature This	
		Review
Relay	Time[s]	Time[s]
R1	0.5482	0.5066
R2	0.6840	0.6163
R3	0.6686	0.4942
R4	0.5826	0.6056
R5	0.4973	0.4750
R6	0.7541	1.1102

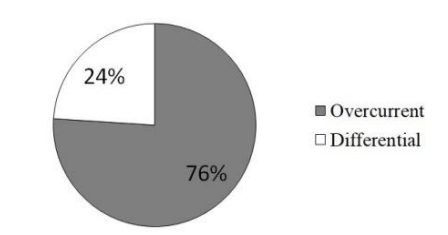


Figure 4. Differential and Overcurrent protection

IV. DISCUSSION AND CONCLUSION

1. Discussion

Although this article carried out the systematic review on coordination of relays in electrical distribution networks it does not lack limitation of the findings. Among the limitation that might have excluded the essential information for coordination of relays could be caused by specifying the year of publication because the year of publication was among the inclusion criteria, there could be best article in the topic under context that could have been excluded due to being out of the specified year of publication.

With reference to the reviewed literatures, for

teleprotection based coordination of relays, it had been reported that the Open Network Operating System controller based on the Software Defined Network had minimum failure occurrence compared to other controllers, which were tested for use in teleprotection. The optimisation of protection relays for the network with 14 protection relays 78.6 % of them were coordinated by an extremely inverse curve [15]. For two different methods; one used the potential energy boundary and another used the bisection, there was a difference of 2.028 cycles [15]. From the reviewed articles the percentage of studies based on differential protection method was 24%, while the percentage studies based on overcurrent relays was 76% as shown in Fig. 3. Most of the differential protection systems were implemented in power transmission lines in which the differential relays installed in transmission substations use the difference in currents to detect the faults while communicating with the remote relays through telecommunication channel. Further the analysis also was carried out moving from the power transmission line to the lower level of the power distribution line, the lower was the percentage of the application of the teleprotection with overcurrent relays. The implication was that there were few studies carried out using teleprotection with overcurrent relays in the power distribution networks.

Based on the type of electrical network; when the benchmark IEC microgrid was used the result of the operating time for the relays had a minimum value of 0.0118s and a maximum value of 1.59s for individual relays [37]. The operating time for individual relays of the network with distributed generators had a minimum of 0.01s and a maximum of 1.3s [15]. The result of operating time for the backup relays in this review had greater spread in values as compared to the result from the literature. The average operating time for backup relays for three bus network was 0.63 seconds with the standard deviation of 0.24 in this review. The literature for comparison had average operating time of 0.62 seconds with the standard deviation of 0.1. The trend of publication on the coordination of relays in electrical distribution networks has been growing and is expected to grow as technology changes and new computational methods keep on evolving. The decentralised adaptive fuzzy based system had good performance compared to enhanced particle swam optimisation when used in the network with distributed generators [15]. The analysis was also carried out to find the extent of the use of the distributed multi agent coordination for relays as compared to other areas of control different from the coordination of relays. Distributed multi agent coordination had been mostly conducted in areas of unmanned aerial vehicles, unmanned ground vehicles, autonomous underwater vehicles, robotics, satellites, and game theory [38-45]. There

are limited articles about the use of distributed leaderless multi agent coordination for coordination of protection relays.

The findings suggest that multi-agent coordination holds significant potential for enhancing the performance and reliability of teleprotection relays in electrical distribution networks. The collaborative nature of multi-agent systems enables efficient fault detection and isolation, leading to improved network resilience and reliability.

2. Conclusion

Most of the publications about the coordination of relays focus on adaptive protection through the use of information and communication technologies to design the coordination techniques capable to make adjust automatically their operational parameter settings according to the changes in the behavior of the electrical network. On the perspective of the use of communication in the protection relays most of the articles published about the coordination of relays mainly focus on the technologies communication that reduce communication delay. Although most of the articles didn't specify communication technologies required for teleprotection; it falls in the category of operational technology and not information technology. In other words, the communication required for protection relays is the operational technology. The operational technology can't tolerate the drop of the message communicated between the devices. In operational technology the dropped message when it was sent becomes useless and no need to push the message in time other than when it was sent. Based on the review it is undoubtedly protection that relavs geographically distributed on the land and they carry out computation of variables, there is a lack of control laws for the multi agent coordination of protection relays in electrical distribution networks. The relays and IEDs in the electrical distribution networks are geographically distributed according to the network of the streets and settlement of the society that uses electrical energy. Modeling the relays and IEDs using multiagent approach is essential to obtain the modern way to control these distributed protection components in the electrical

REFERENCES

[1] B. Lundqvist, "100 years of relay protection, the Swedish ABB relay history," Västerås, 2001. [Cited 10/12/2023]. http://library.abb.com/global/scot/scot296.n sf/veritydisplay/c1256d32004634bac1256e 19006fd705/\$File/PAPER 2001 08 en 10 0 Years of Relay Protection the Swedi sh_ABB_Relay_History.pdf.

network.

This systematic review provides a comprehensive overview of the current state of research on the application of multi-agent coordination for teleprotection relays in electrical distribution networks. The findings highlight the potential benefits of utilizing multi-agent coordination in enhancing fault detection accuracy, reducing communication delays, and improving the overall reliability of teleprotection relay systems. In this paper, a systematic review was carried out and obtained the findings from various studies, on the coordination of relays in terms of operating time of protection relays in electrical distribution networks. Findings used the available data to build on the evidence about various techniques in coordination of relays. The findings incorporated the requirements for innovation in the coordination of relays in the protection of the electrical network. It was evident from the review that most of the studies concerning multi agent coordination had been carried out in other areas different from protection relays. Also, the review found that the studies that reported about the coordination of protection relays had limited coverage of the distributed control rules. Therefore, there is limited research on distributed control rules of the multi agent coordination of protection relays.

V. AUTHOR CONTRIBUTIONS

Godfrey Mhagama: Conceptualization, Literature review, Theoretical analysis, Writing.

Ndyetabura Y. Hamisi: Supervision, Review and editing.

Shililiandumi Naiman: Supervision, Review and editing.

VI. DISCLOSURE STATEMENT

The authors declare that they have no known competing financial interests or personal relationships that could have appeared to influence the work reported in this paper.

ORCID

G Mhagama https://orcid.org/0000-0002-0941-9006

- [2] A. J. Urdaneta, R. Nadira, and L. G. Pérez Jiménez, "Optimal Coordination of Directional Overcurrent Relays in Interconnected Power Systems," *IEEE Trans. Power Deliv.* 3 (3) (1988) pp. 903–911. https://doi.org/10.1109/61.193867
- [3] T. Amraee, "Coordination of directional overcurrent relays using seeker algorithm,"

- *IEEE Trans. Power Deliv.* 27 (3) (2012) pp. 1415–1422.
- https://doi.org/10.1109/TPWRD.2012.2190 107
- [4] Z. N. Stojanovic and M. B. Djuric, "Table Based Algorithm for Inverse-Time Overcurrent Relay," *J. Electr. Eng.* 65 (4) (2014) pp. 213–220. https://doi.org/10.2478/jee-2014-0033
- [5] A. Srivastava, J. M. Tripathi, S. R. Mohanty, and B. Panda, "Optimal over-current relay coordination with distributed generation using hybrid particle swarm optimization-gravitational search algorithm," *Electr. Power Components Syst.* 44 (5) (2016) pp. 506–517. https://doi.org/10.1080/15325008.2015.111
- [6] M. H. Costa, R. R. Saldanha, M. G. Ravetti, and E. G. Carrano, "Robust coordination of directional overcurrent relays using a matheuristic algorithm," *IET Gener. Transm. Distrib.* 11 (2) (2017) pp. 464–474. https://doi.org/10.1049/iet-gtd.2016.1010

7539

- [7] S. Roy, S. B. Perli, and N. V. P. Babu, "Intelligent coordination of overcurrent and distance relays using meta heuristic algorithms," *Int. J. Electr. Eng. Informatics* 10 (4) (2018) pp. 675–703. https://doi.org/10.15676/ijeei.2018.10.4.5
- [8] A. Korashy, S. Kamel, F. Jurado, and A. R. Youssef, "Hybrid Whale Optimization Algorithm and Grey Wolf Optimizer Algorithm for Optimal Coordination of Direction Overcurrent Relays," *Electr. Power Components Syst.* 47 (6–7) (2019) pp. 644–658.
 - https://doi.org/10.1080/15325008.2019.160 2687
- [9] M. Y. Shih, A. Conde, and C. Ángeles-Camacho, "Enhanced self-adaptive differential evolution multi-Objective algorithm for coordination of directional overcurrent relays contemplating maximum and minimum fault points," *IET Gener. Transm. Distrib.*, 13 (21) (2019) pp. 4842–4852.
 - https://doi.org/10.1049/iet-gtd.2018.6995
- [10] B. Dumala, "Optimal Coordination of Over Current Relays Using Teaching Learning Based Optimization Algorithm" 4 (3) (2020) pp. 10–20.
- [11] T. A. W. Mykel J.Kochenderfer, *Algorithms* for *Optimization*, Cambridge: MIT Press, 2019.
- [12] R. V Rao, V. J. Savsani, and D. P. Vakharia, "Computer-Aided Design Teaching – learning-based optimization: A novel method for constrained mechanical design optimization problems," *Comput. Des.* 43

- (3) (2011) pp. 303–315. https://doi.org/10.1016/j.cad.2010.12.015
- [13] S. Beheshtaein, R. Cuzner, M. Savaghebi, and J. M. Guerrero, "Review on microgrids protection," *IET Gener. Transm. Distrib.* 13 (6) (2019) pp. 743–759. https://doi.org/10.1049/iet-gtd.2018.5212
- [14] A. Alvarez de Sotomayor, D. Della Giustina, G. Massa, A. Dedè, F. Ramos, and A. Barbato, "IEC 61850-based adaptive protection system for the MV distribution smart grid," *Sustain. Energy, Grids Networks* 15 (October) (2018) pp. 26–33. https://doi.org/10.1016/j.segan.2017.09.003
- [15] A. E. C. Momesso, W. M. Wellington, and E. N. Asada, "Adaptive directional overcurrent protection considering stability constraint," *Electr. Power Syst. Res.* 181 (December) (2019) p. 106190. https://doi.org/10.1016/j.epsr.2019.106190
- [16] B. J. Brearley, R. Raja Prabu, K. Regin Bose, and V. Sankaranarayanan, "Adaptive relay co-ordination scheme for radial microgrid," *Int. J. Ambient Energy* 43 (1) (2020) pp. 2180-2193. https://doi.org/10.1080/01430750.2020.172
- [17] S. T. P. Srinivas and K. Shanti Swarup, "A New Mixed Integer Linear Programming Formulation for Protection Relay Coordination Using Disjunctive Inequalities," *IEEE Power Energy Technol. Syst. J.* 6 (2) (2019) pp. 104–112. https://doi.org/10.1109/jpets.2019.2907320
- [18] M. Dolatabadi and Y. Damchi, "Graph Theory Based Heuristic Approach for Minimum Break Point Set Determination in Large Scale Power Systems," *IEEE Trans. Power Deliv.* 34 (3) (2019) pp. 963–970. https://doi.org/10.1109/TPWRD.2019.2901 028
- [19] B. M. Buchholz and Z. Styczynski, *Smart grids Fundamentals and technologies in electricity networks*, vol. 9783642451. Springer Berlin Heidelberg, 2014.
- [20] M. G. Maleki, H. Javadi, M. Khederzadeh, and S. Farajzadeh, "An Adaptive and Decentralized Protection Scheme for Microgrid Protection," *Power Syst. Prot. Control Conf. (PSPC)*, *Tehran, Iran*, no. July, 2016. https://doi.org/10.20944/preprints201907.0 251.v1
- [21] M. J. Daryani, A. E. Karkevandi, and O. Usta, "Multi-Agent Approach to Wide-Area Integrated Adaptive Protection System of Microgrid for Pre-and Post-Contingency Conditions," Proc. 2018 IEEE PES Innov. Smart Grid Technol. Conf. Eur. ISGT-Europe 2018, pp. 1–6.

- https://doi.org/10.1109/ISGTEurope.2018.8 571785
- [22] M. S. Rahman, T. F. Orchi, S. Saha, and M. E. Haque, "Multi-Agent Approach for Overcurrent Protection Coordination in Low Voltage Microgrids," *IEEE Power Energy Soc. Gen. Meet.*, vol. 2019-Augus, 2019. https://doi.org/10.1109/PESGM40551.2019.8974053
- [23] X. Tong *et al.*, "The study of a regional decentralized peer-to-peer negotiation-based wide-area backup protection multi-agent system," *IEEE Trans. Smart Grid* 4 (2) (2013) pp. 1197–1206. https://doi.org/10.1109/TSG.2012.2223723
- [24] Z. Liu, C. Su, H. K. Hoidalen, and Z. Chen, "A Multiagent System-Based Protection and Control Scheme for Distribution System with Distributed-Generation Integration," IEEE Trans. Power Deliv. 32 (1) (2017) pp. 536–545. https://doi.org/10.1109/TPWRD.2016.2585 579
- [25] Z. Liu, Z. Chen, H. Sun, and Y. Hu, "Multi agent system based process control in wide area protection against cascading events," 2013 IEEE Grenoble Conf. PowerTech, POWERTECH 2013, pp. 445–450. https://doi.org/10.1109/PTC.2013.6652293
- [26] M. Singh, B. K. Panigrahi, and A. R. Abhyankar, "A hybrid protection scheme to mitigate the effect of distributed generation on relay coordination in distribution system," *IEEE Power Energy Soc. Gen. Meet.*, pp. 13–17, 2013. https://doi.org/10.1109/PESMG.2013.6672
- [27] K. I. Tharakan, P. Sasikumar, and C. Vaithilingam, "Wireless protective relaying for smart grid," *ARPN J. Eng. Appl. Sci.* 11 (21) (2016) pp. 12756–12759.
- [28] A. Yadav and A. Swetapadma, "Improved first zone reach setting of artificial neural network-based directional relay for protection of double circuit transmission lines," *IET Gener. Transm. Distrib.* 8 (3) (2014) pp. 373–388. https://doi.org/10.1049/iet-gtd.2013.0239
- [29] O. Nunez, F. Valencia, P. Mendoza-Araya, R. Palma-Behnke, G. Jimenez, and J. Cotos, "Microgrids protection schemes," CHILECON 2015 2015 IEEE Chil. Conf. Electr. Electron. Eng. Inf. Commun. Technol. Proc. IEEE Chilecon 2015, no. November, pp. 597–602, 2016. https://doi.org/10.1109/Chilecon.2015.7400 439
- [30] H. Karimi, G. Shahgholian, B. Fani, I. Sadeghkhani, and M. Moazzami, "A protection strategy for inverter-interfaced

- islanded microgrids with looped configuration," *Electr. Eng.* 101 (3) (2019) pp. 1059–1073. https://doi.org/10.1007/s00202-019-00841-
- [32] S. Panneer, J. R. Meenakshi, and S. Bharti, "Practice A Methodology for Sustainable Models in the Helping Professions," *Soc. Work Educ. Res. Pract. Univ. Tamil Nadu*, pp. 161–172, 2020. https://doi.org/10.1007/978-981-15-9797-8 12
- [33] D. Kusumaningsih, "Mendeley As A Reference Management and Citation Generator for Academic Articles," *Adv. Eng. Res.* 175 (ICASE-18) (2018) pp. 81–83. https://doi.org/10.2991/icase-18.2018.22
- [34] T. Khurshaid, A. Wadood, S. Gholami Farkoush, J. Yu, C. H. Kim, and S. B. Rhee, "An Improved Optimal Solution for the Directional Overcurrent Relays Coordination Using Hybridized Whale Optimization Algorithm in Complex Power Systems," *IEEE Access* 7 (2019) pp. 90418–90435.

 https://doi.org/10.1109/ACCESS.2019.292
 5822
- [35] K. Sarwagya, P. K. Nayak, and S. Ranjan, "Optimal coordination of directional overcurrent relays in complex distribution networks using sine cosine algorithm," *Electr. Power Syst. Res.* 187 (2020) p. 106435. https://doi.org/10.1016/j.epsr.2020.106435
- [36] S. D. Saldarriaga-Zuluaga, J. M. López-Lezama, and N. Muñoz-Galeano, "Optimal coordination of over-current relays in microgrids considering multiple characteristic curves," *Alexandria Eng. J.* 60 (2) (2021) pp. 2093–2113. https://doi.org/10.1016/j.aej.2020.12.012
- [37] S. D. Saldarriaga-Zuluaga, J. M. López-Lezama, and N. Muñoz-Galeano, "An Approach for Optimal Coordination of Over-Current Relays in Microgrids with Distributed Generation," *Electronics* 9 (10) (2020) p. 1740. https://doi.org/10.3390/electronics9101740
- [38] G. Wang, C. Wang, X. Cai, and Y. Ji, "Distributed Leaderless and Leader-Following Consensus Control of Multiple Euler-Lagrange Systems with Unknown Control Directions," J. Intell. Robot. Syst.

- *Theory Appl.* 89 (3–4) (2018) pp. 439–463. https://doi.org/10.1007/s10846-017-0554-1
- [39] M. Rehan, M. Tufail, and S. Ahmed, "Leaderless consensus control of nonlinear multi-agent systems under directed topologies subject to input saturation using adaptive event-triggered mechanism," *J. Franklin Inst.* 358 (12) (2021) pp. 6217–6239.

 https://doi.org/10.1016/j.jfranklin.2021.06.0
- [40] M. M. Eissa, "New protection philosophy for protecting complex smart grid with renewable resources penetration," 2012 IEEE Int. Conf. Smart Grid Eng. SGE 2012, 2012.
- https://doi.org/10.1109/SGE.2012.6463966

 Z. Lin, L. Wang, Z. Han, and M. Fu, "Distributed formation control of multiagent systems using complex laplacian," *IEEE Trans. Automat. Contr.*, 59 (7) (2014) pp. 1765–1777. https://doi.org/10.1109/TAC.2014.2309031

- [42] Z. Yang, X. Pan, Q. Zhang, and Z. Chen, "Formation control of first-order multiagents with region constraint," *Automatika* 61 (4) (2020) pp. 651–656.

 https://doi.org/10.1080/00051144.2020.181 4979
- [43] Q. Wang, Y. Wang, and H. Zhang, "The formation control of multi-agent systems on a circle," *IEEE/CAA J. Autom. Sin.* 5 (1) (2018) pp. 148–154. https://doi.org/10.1109/JAS.2016.7510022
- [44] S. L. Bowman, C. Nowzari, and G. J. Pappas, "Coordination of multi-agent systems via asynchronous cloud communication," 2016 IEEE 55th Conf. Decis. Control. CDC 2016, pp. 2215–2220. https://doi.org/10.1109/CDC.2016.7798592
- [45] Q. Wang, H. Gao, F. Alsaadi, and T. Hayat, "An overview of consensus problems in constrained multi-agent coordination," *Syst. Sci. Control Eng.* 2 (1) (2014) pp. 275–284. https://doi.org/10.1080/21642583.2014.897



This article is an open access article distributed under the terms and conditions of the Creative Commons Attribution NonCommercial (CC BY-NC 4.0) license.